Disposable *Smart* Lab on a Chip for Point-of-Care Clinical Diagnostics

CHONG H. AHN, JIN-WOO CHOI, GREGORY BEAUCAGE, JOSEPH H. NEVIN, MEMBER, IEEE, JEONG-BONG LEE, ANIRUDDHA PUNTAMBEKAR, AND JAE Y. LEE

Invited Paper

This paper presents the development of a disposable plastic biochip incorporating smart passive microfluidics with embedded on-chip power sources and integrated biosensor array for applications in clinical diagnostics and point-of-care testing. The fully integrated disposable biochip is capable of precise volume control with smart microfluidic manipulation without costly on-chip microfluidic components. The biochip has a unique power source using on-chip pressurized air reservoirs, for microfluidic manipulation, avoiding the need for complex microfluidic pumps. In addition, the disposable plastic biochip has successfully been tested for the measurements of partial oxygen concentration, glucose, and lactate level in human blood using an integrated biosensor array. This paper presents details of the smart passive microfluidic system, the on-chip power source, and the biosensor array together with a detailed discussion of the plastic micromachining techniques used for chip fabrication. A handheld analyzer capable of multiparameter detection of clinically relevant parameters has also been developed to detect the signals from the cartridge type disposable biochip. The handheld analyzer developed in this work is currently the smallest analyzer capable of multiparameter detection for point-of-care testing.

Keywords*—*Biosensor array, clinical diagnostics, lab on a chip, on-chip power source, smart passive microfluidics.

I. INTRODUCTION

The development of lab-on-a-chip devices for biochemical analysis has seen an explosive growth over the past decade. Initial research in this area focused on developing the concepts of micro total analysis systems (μTAS), a parallel term to "lab on a chip," and has rapidly evolved to applications in a number of biochemical analysis operations such as clinical analysis (blood gas analysis, glucose/lactate analysis, etc.), DNA analysis (including nucleic acid sequence analysis), proteomics analysis (proteins and peptides), combinatorial synthesis/analysis, immunoassays, toxicity monitoring, and even forensic analysis applications [1]–[9]. A significant application area for this technology is clinical diagnostics. Specifically for clinical diagnostics, diseases, including toxicity, can be diagnosed by performing various biochemical analyzes and by observation of symptoms. The early, rapid, and sensitive detection of the disease state is a vital goal for clinical diagnoses. The biochemical changes in the patient's blood can signal organ damage or dysfunction prior to observable microscopic cellular damages or other symptoms. So there has been a large demand for the development of an easy-to-handle and inexpensive clinical diagnostic biochip using fully integrated plastic microfluidic chips, which has the sampling/identifying capability of fast and reliable measurements of metabolic parameters from a human body with minimum invasion.

Most clinical diagnostics applications have focused on the detection of nucleotides and peptides that serve as early indicators of disease [1], [3], [10], [11]. For instance, Dinh *et al.* describe a multifunctional biochip with nucleic acid and antibody probe receptors specific to the gene fragments of *Bacillus anthracis* and *Escherichia coli*, respectively [10]. The detection of specific diseases or biological warfare agents is possible by incorporating biomarkers specific to such agents. Clinical diagnostic applications also include monitoring of regular metabolic parameters such as *glucose* and *lactate* as demonstrated by the I-Stat analyzer. The handheld analyzer provides point-of-care testing for monitoring a variety of clinically relevant parameters [12]. Immunosensing applications as a part of clinical diagnostics have also been demonstrated [13], [14].

Manuscript received March 15, 2003; revised June 29, 20003. This work was supported by the Defense Advanced Research Projects Agency under Contract AF F30602-00-1-0569 from the BioFlips program, U.S. Department of Defense.

C. H. Ahn, G. Beaucage, J. Nevin, and A. Puntambekar are with the University of Cincinnati, Cincinnati, OH 45221 USA (e-mail: chong.ahn@uc.edu).

J.-W. Choi is with the Louisiana State University, Baton Rouge, LA 70801 USA.

J. B. Lee is with the University of Texas at Dallas, Richardson, TX 75083 USA.

J. Y. Lee is with the Ohio State University, Columbus, OH 45221 USA.

Digital Object Identifier 10.1109/JPROC.2003.820548

The range of applications for lab-on-a-chip systems is increasingly rapidly as more and more researchers become aware of the significant benefits of this technology. Most of these advantages are derived from the small sample and reagent volume utilized in these systems [8], [15], [16].

The advantages include low sample/reagent volume, rapid analysis times, less sample wastage, cost effectiveness (for sample usage), and possibility of developing disposable devices to name a few. Though the analyte can be manipulated in various physical forms such as liquid stream [1], liquid droplets [8], and gaseous phase [6], microfluidic biochemical analysis (using liquid streams) have been the primary focus of research efforts. One of the more significant challenges in developing a microfluidic biochemical analysis system has been the development of reliable microfluidic manipulation techniques. Various researchers have explored active control devices such as microvalves and micropumps for fluidic flow control [17]–[27]. However, active microfluidic control has certain inherent disadvantages such as high cost, difficulty in integration, complex fabrication/assembly, and complex control circuitry.

Increasingly researchers are shifting their attention toward the use of passive microfluidic structures to regulate microfluidic sequencing. A large number and variety of passive microfluidic devices have been successfully demonstrated including passive valves [28]–[35], mixers [36]–[40], diffusion-based extractors [41], [42], passive filters and membranes [43], [44], and also a few passive actuation schemes [45]–[47]. Passive microfluidic devices (or systems) offer some advantages specifically for biochemical analysis systems such as no external power requirement (for device operation), ease of integration, continuity in substrate material, rapid prototyping, low cost, and possibility of use without active control. Some of the challenges facing passive microfluidic devices/systems are that passive microfluidic systems are very application specific; they cannot be easily reconfigured; and they are strongly dependent on variances in the fabrication process and are not suitable for a wide range of fluidic mediums. Despite these challenges, the advantages of the passive control approach make it a viable approach for developing microfluidic platforms for biochemical analysis.

One of the most critical decisions for a μTAS platform is the choice of substrate material. Most microfluidic biochemical analysis systems have been fabricated using silicon (Si) or glass as substrates for the microfluidic motherboards. There is considerable effort toward exploring substrates other than Si or glass, primarily toward plastic/polymer-based motherboards [48]–[55]. Plastic substrates, such as polyimide, polymethamethylacrylate (PMMA), poly(dimethylsiloxane) (PDMS), polyethylene, or polycarbonate, offer a wide range of physical and chemical material parameters for the applications of biofluidic chips generally at low cost using replication approaches. Polymers offer numerous advantages like low cost, rugged construction, ease of fabrication, and rapid prototyping. A significant advantage of using polymer substrates is the wide variety of surface properties that they offer. The surface properties of polymers can be readily modified to meet the fluidic and/or biocompatibility requirements of the biochemical analysis system [56], [57]. Also, polymer processing is a mature, established science and μTAS researchers can readily exploit the significant data bank of the polymer experts to create multifunctional, low-cost, disposable microfluidic modules.

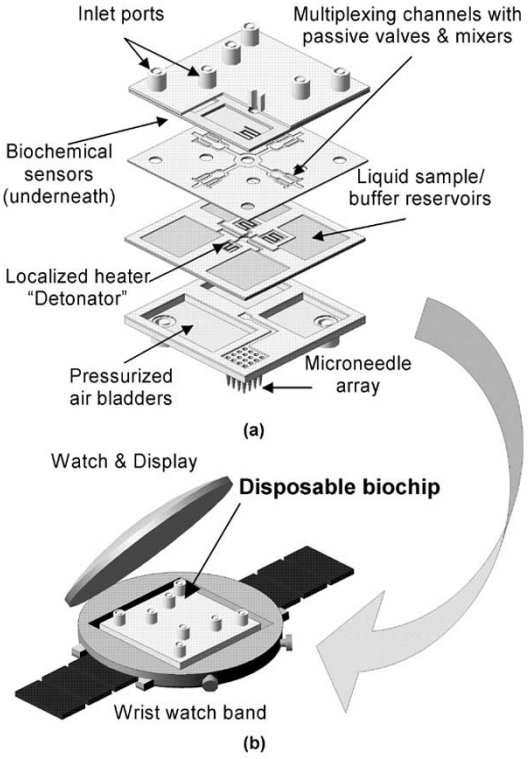

Fig. 1. Schematic sketch showing: (a) details of multilayer plastic disposable biochip and (b) wristwatch analyzer for detecting point-of-care testing with biochip.

In this paper, the development of disposable smart plastic fluidic biochips for clinical diagnostics is reviewed. Fig. 1 shows a schematic sketch of the disposable lab on a chip with wristwatch-sized analyzer. The plastic fluidic chip includes a smart passive microfluidic manipulation system based on the structurally programmable microfluidic system (sPROMs) technology, allowing for preprogrammed sets of microfluidic sequencing with only an on-chip pressure source.

The integration of the air-bursting detonator allows us to utilize a simple alternative fluid-driving source, thus eliminating costly, nondisposable active microfluidic pumps. The biochip also contains an integrated biosensor array for simultaneous detection of multiple clinically relevant parameters. Thus, the disposable smart plastic biochip is composed of fully integrated modules of plastic fluidic chips for fluid driving, sequencing, and biochemical sensors. The biochip is inserted into the analyzer unit where the microfluidic sequencing is initiated by a trigger signal from the electronic controller. After the sample solution (blood) is delivered to the biosensor array, the electrochemical detection circuitry on the analyzer is used to determine the concentrations of the various analytes. As a demonstration vehicle, the biochip has the specific goal to detect and identify three metabolic parameters: PO_2 (partial pressure of oxygen), *lactate*, and *glucose* from blood.

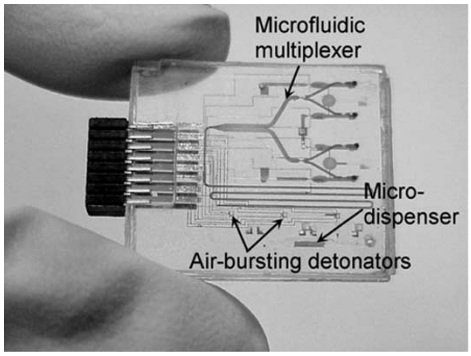

Fig. 2. Assembled biochip with sPROMs-based microfluidic control system and air-bursting detonators for fluid driving.

II. Disposable *Smart* Lab on a Chip

The development of a disposable, smart lab on a chip (or biochip) requires considerable research effort toward developing a clear understanding of the various components of the biochip. These include the microfluidic system, the biosensor arrays, and the fabrication techniques required to implement these in a feasible and economically viable fashion.

The use of stand-alone μTAS devices for remote and/or portable systems requires the development of a microfluidic control modality that can function reliably with minimal control signals. We have concentrated on the development of the sPROMs technology that offers the following features—passive fluidic manipulation, low-volume handling capability, low actuation power, low cost, disposability, robustness, and little or no feedback control. Furthermore, sPROMs devices with no moving parts are inherently more rugged and less fault prone. Since sPROMs-based devices can be readily implemented on low-cost plastic substrates, this technology is highly suitable for disposable microfluidic platform applications. Finally, this technology allows us to manipulate ultrasmall volumes [typically in the nanoliter (nL) to microliter $(\mu\mathrm{L})$ range] of fluids, thus exploiting maximum advantage of the μTAS concept. We have extensively developed the sPROMs technology to realize devices such as microfluidic multiplexers with integrated microdispenser that allows the transfer of precise aliquots of fluid from a single input to multiple outputs in a programmed sequence.

This arrangement can then be extended to handle minute samples of multiple fluids simultaneously as a first step toward realizing a complete biochemical analysis system on chip. Fig. 2 shows an assembled biochip with the sPROMs-based multiplexer and integrated dispenser. A detailed operation of this device is presented later in the paper.

Another critical element of the biochip is the on-chip air-bursting detonator. The air-bursting detonator uses pressurized gas, which is compressed and stored in a chamber capped with a thin membrane. The membrane has a heater lithographically defined to serve as the detonator. When a brief pulse of electrical energy is sent to the microheater, the heater temperature rises rapidly and melts the membrane. As soon as the membrane is broken the pressurized gas rushes out, pushing the fluid samples into the microchannel through the ruptured membrane. Low power consumption is guaranteed, since only pulsed power is used to burst the pressurized gas. This eliminates the use of complex micropumps as well as bulky batteries required to power the pumps.

The use of a smart passive microfluidic control system with an on-chip power source allows for the development of fully integrated, yet low-cost disposable biochips. The following sections present detailed information about various aspects of the biochip design, fabrication, and characterization.

A. Materials

This section covers the plastic micromachining part of the biochip that is integral for the successful development of a plastic biochip.

1) Choice of Plastic Substrate: An important factor in the biochip design and implementation is the choice of the plastic substrate. As listed previously a wide variety of plastic substrates are available for biochip fabrication. Most commonly polycarbonate (PC) and PMMA have been used as substrate materials. Though PC and PMMA offer certain attractive characteristics for bio-microelectromechanical systems (bioMEMS) applications, we have chosen cyclic olefin copolymers (COC), as it offers significantly better material properties. COC is a relatively new polymer material and is highly suitable for the biochip application.

Some of the advantages of using COC include the following.

- COC can be injection molded at very high flow rates ($\sim$55 g per 10 min) compared to other polymer materials. PC and PMMA can only be injected at 27 g and 25 g per 10 min, respectively. The lower viscosity of COC at processing temperatures allows for lower injection pressure and better fills.
- COC exhibits extremely low water absorption, typically an order of magnitude lower than PC or PMMA.
- Most metallic films exhibit excellent adhesion to the COC substrate.
- COC is resistant to most polar solvents such as acetone, methanol, and iso-propyl alcohol. This allows the use of standard photolithography techniques with COC substrates.
- A significant advantage is the wide UV transmittance exhibited by COC. Fig. 3 shows the UV transmittance characteristics of COC compared with PC and PMMA. COC has excellent optical properties, which are advantageous for fluorescein-based biochemical analyzes and biooptical applications [58].

2) Plastic Micromachining Using the Replaceable Mold Disk Technique: A wide variety of techniques such as hot embossing, casting, and injection molding have been used previously for plastic replication. Of the above listed techniques, injection molding has very short process times and is well suited for a mass-production approach. Conventional injection molding techniques involve injection of molten polymer in a molding block that contains the

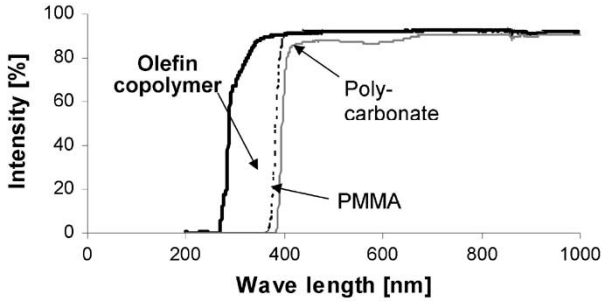

Fig. 3. Measured optical transparency and absorption characteristics for different wavelengths after injection. UV range is transparent for olefin copolymers.

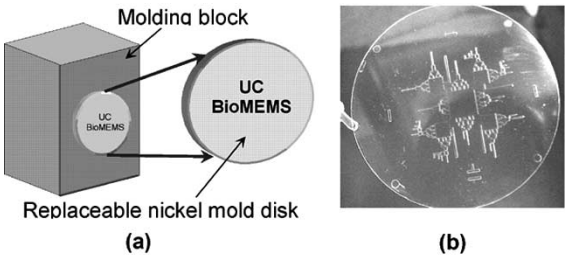

Fig. 4. (a) Replaceable mold disk technique using custom designed molding block. (b) Molded plastic wafer.

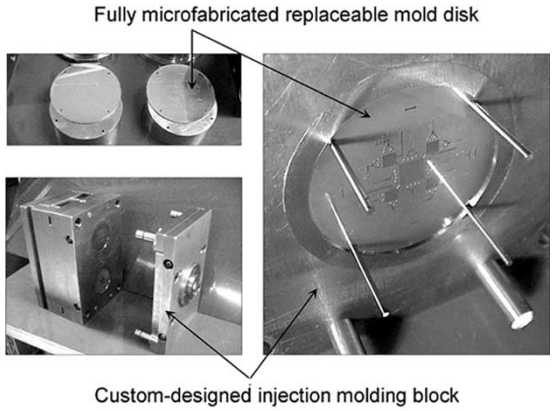

Fig. 5. Photographs of the custom designed molding block with the replaceable Ni mold disk and the fabricated microstructures in the Ni mold disk insert.

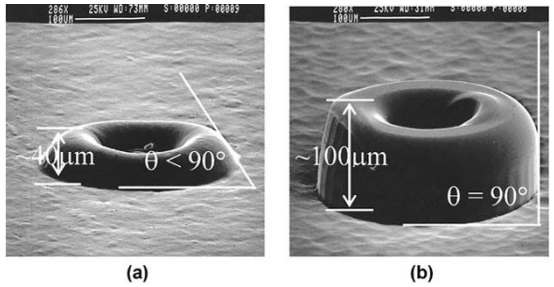

Fig. 6. SEM images of high aspect ratio microstructures. (a) Without RTP process. (b) With RTP process.

patterns to be replicated. The injection molding block is a critical component if the molding system and is also a fairly expensive component. There has been a clear need to develop a low-cost, rapid turnaround time technique for the mold manufacturing.

We have developed a novel replaceable mold disk technique to address this problem. In this technique, the high-aspect ratio microstructures are fabricated on a circular nickel disk about 3 in in diameter and 1.5 mm in thickness. The disk is inserted in the molding block, as shown in Fig. 4(a) and (b) shows an image of the injection molded plastic wafer. The mold disk can be taken out from the molding block and be replaced with any other pattern without replacing the whole molding block [59].

The replaceable mold disk technique is also suitable for use with existing microfabrication techniques, which allows the replaceable molding technique to be a highly economically viable technique. Fig. 5 shows the actual custom designed molding block that can be used together with the replaceable molding disk to create microstructured plastic wafers.

3) Rapid Thermal Process (RTP) for Injection Molding: In a typical injection molding process, the plastic is melted and then injected into the cavity of a closed mold, whose shape is transferred to plastic microstructures on cooling down. Inside the mold cavity, the resin continues to flow and fill the mold cavity till the polymer cools down to a highly viscous melt, where the flow stops, and the part can be ejected. In order to ensure good flow properties during injection, thermoplastics with low or medium viscosity are preferred. So the filling of the mold cavity and subsequently the micro patterns depend on viscosity of polymer melt, injection speed, molding block temperature, and the nozzle temperature of the injection unit.

The molding block is normally heated to an elevated temperature (below glass transition temperature of the injected polymer) to help uniform flow of polymer throughout the mold cavity. A higher mold temperature could improve the fill characteristics but would also significantly increase the process time.

In the rapid thermal process, the "surface" of a Ni mold disk is heated with IR radiation using a high power halogen lamp. The radiation from the IR source is focused to the surface of the Ni disk, which heats up to a high temperature in a few seconds. Then, the molding block is closed and the molten plastic is injected from the nozzle at high injection speeds. When the molten plastic enters the mold cavity, it experiences an isothermal environment. The melt temperature and the Ni mold disk surface temperature will be the same at the instant when the plastic is injected. So there will be no heat transfer taking place inside the cavity for a very small period and the surface heat of the Ni mold disk will help the plastic to be in a state of low viscosity. As a result of this, complete filling of the mold disk cavity can be achieved without a considerable increase in the cycle time of operation of the injection mold machine [60].

Scanning electron microscopy (SEM) images of a high-aspect ratio microstructure are shown in Fig. 6. The shape of the microstructure without the RTP process is that of a partially filled micro cavity, where the plastic has solidified before complete filling of the mold cavity. The structure shown

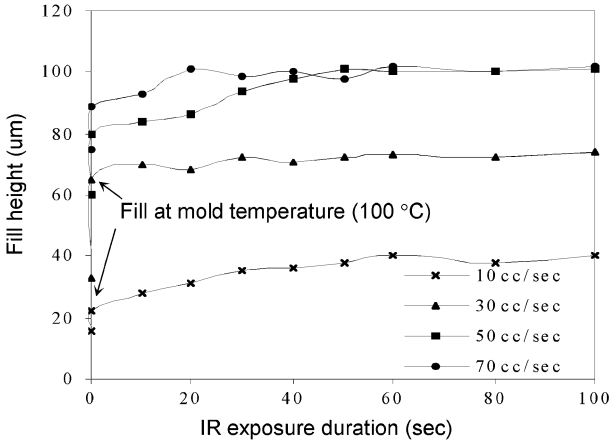

Fig. 7. Measured injection fill depths at various IR exposure times, flow rates, and molding block temperatures for COC.

in Fig. 6(b), using the RTP process shows complete filling of the mold and good replication of the microstructure in the mold cavity. The height of the plastic structure is around 100 μm, which is the depth of the micro cavity in the mold and the sidewall also has an angle of almost 90°, ensuring exact replication of the mold cavity.

The characterization results of the RTP process are summarized in Fig. 7. The height of the micromold used for these experiments was 100 μm and effects of IR radiation (i.e., higher molding block temperature) can be seen clearly.

4) Surface Modification of COC Substrate: For most bioMEMS applications, the surface characteristics (glass transition temperature, nonspecific adsorption, free surface energy, etc.) of a plastic substrate are usually of greater interest than the bulk properties of the plastic material. From a fabrication perspective, the bulk properties of the plastic (rigidity, mechanical strength, etc.) are also important.

The native surface of a COC plastic wafer exhibits a contact angle of $\sim 92^{\circ}$ with water. For sPROMs applications, as described later, it is essential to have a strongly hydrophobic surface. Thus, it is essential to modify the surface of the COC wafer to achieve the high hydrophobicity. In this work, we have chosen plasma treatment, with reactive ion etching (RIE) techniques to modify the surface of the COC substrate. The surface modification should affect the surface free energy (and in turn the contact angle) as well as the biocompatibility characteristics of the COC substrates.

Plasma processing was chosen for this application because it is a well-established technique for surface modification. Plasma processing is widely used for MEMS applications such as dry etching, and is a familiar technique for most MEMS engineers. Plasma treatment can also modify the surface characteristics over nonuniform surfaces such as plastic wafer with channels on it. Finally, this technique is well suited for the batch fabrication approach and maintains the low-cost requirement for a disposable biochip.

Table 1 shows the plasma processing conditions used to modify the surface characteristics of the COC substrate. The conditions were chosen such that there was very little $(<15^{\circ})$ change in contact angle after thermal cycling of the COC samples. During the thermal cycling tests, the plasma treated

Table 1
Plasma Processing Conditions for Surface Modification of COC Substrate

Case #	[Flow Rate] Ar (sccm)	O_2 (sccm)	CF_4 (sccm)	Power (Watts)	Duration (seconds)	Contact angle (degree)
1	20	0	0	200	120	~5°
2	10	0	0	150	120	21°
3	10	0	0	100	120	48°
4	10	0	0	25	120	78°
5	0	0	10	100	120	100°
6	0	2	10	150	120	109°
7	0	3	10	150	120	122°
8	0	4	10	200	120	136°

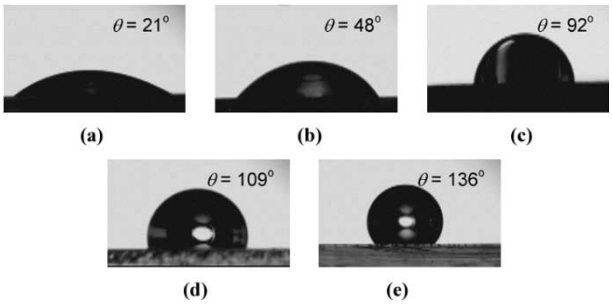

Fig. 8. Contact angle measurement results for: (a) case 2; (b) case 3; (c) *native COC;* (d) case 6; and (e) case 8 as listed in Table 1.

samples were heated to 120 °C and cooled down to verify the stability of the surface modification [61].

Fig. 8 shows the results of the plasma modification verified by measuring water contact angle angles with a goniometer. We have also tried using oxygen plasma to generate hydrophilic surfaces. With oxygen plasma, it is very difficult to control the contact angle even with short duration plasma. Typically, the contact angle drops from 92° to $\sim 20^{\circ}$ even with a short-duration O_2 plasma. Hence, an argon plasma was chosen to achieve the desired the control of contact angle. As case numbers 5–8 in Table 1 show, to generate a hydrophobic surface, we have used a combination of oxygen and carbon tetrafluoride (CF_4) plasma. Using CF_4 plasma alone does not result in the desired increase in contact angle. We believe that in this case, the more energetic oxygen atoms could be knocking out a greater number of surface C–H (or CH_2) bonds as compared to CF_4 plasma alone. Since fluorine is a more reactive species, it would then have a greater number of binding sites open, which may explain the higher hydrophobicity.

The surfaces of the plasma-modified surfaces were examined with attenuated total reflectance (ATR) technique. Fig. 9 shows the ATR spectrum of an oxygen plasma treated COC sample and a $(O_2 + CF_4)$ plasma treated sample, compared with native COC spectrum. Fig. 9(a) shows the effect of combined $(CF_4 + O_2)$ plasma on the COC surface. The native COC surface has a strong CH_2 peak and a smaller C–H peak. After plasma treatement, both the peaks are almost completely wiped out and replaced by a C–F peak and a C=O (ketone) peak. The C–F peak is significantly more dominant and can explain the higher hydrophobicity of the substrate.

Fig. 9(b) shows the effects of oxygen plasma. As shown in Fig. 9(b), the CH_2 peak and C–H peak are both reduced in

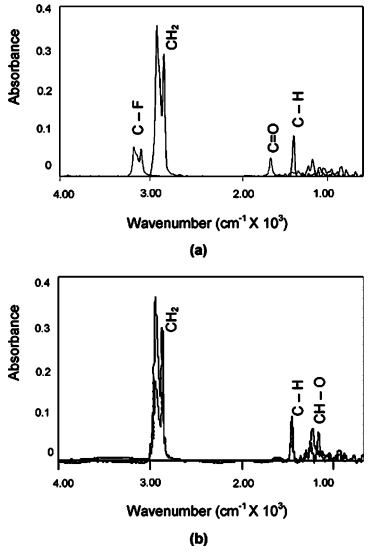

Fig. 9. ATR spectra. (a) COC substrate before and after treatment with $CF_4 + O_2$ plasma. (b) Before and after treatment with O_2 plasma.

magnitude and a new CH–O peak is seen. The polar nature of the (CH–O) can explain the increase in hydrophilic behavior of the substrate. Thus, by choosing the appropriate gases for plasma, power and duration, we can predictably modify the surface of the plastic (COC) substrate across a wide spectrum of contact angles ranging from very hydrophilic $(\sim 5^\circ)$ to very hydrophobic (136°).

5) Thermoplastic Fusion Bonding: A key process in developing a multilayer biochip configuration is the successful implementation of an assembly scheme that can provide leak-free sealing without any deformation of the microstructures. We have extensively investigated thermoplastic fusion bonding for assembly of the biochip. Thermoplastic fusion bonding offers certain distinct advantages for biochip assembly: the bond strength is usually very high, under optimized conditions the deformation can be minimized, and most importantly, it does not involve a foreign substance such as epoxy for assembly.

We have developed a novel low-temperature bonding process whereby the temperature of the COC substrate is maintained ∼20°–40°C below T_g (glass transition temperature). Instead a very high pressure is applied to force the two samples in contact. At high pressures (tens of megapascals) the two samples are well bonded. The bond strength is enough to ensure that there is no fluidic leakage around the microchannels. More importantly, the low-temperature bonding minimizes the deformation of the microchannels substantially [61].

Fig. 10 shows a four-layer microfluidic network assembled using thermoplastic fusion bonding. The three distinct fluidic layers can be easily visualized because the color of the liquid in a branch is the same before and after it crosses liquid in another branch. This is only possible if the three liquids are on different planes, i.e., stacked on top of each other.

Fig. 11 shows a cross-sectional SEM of the bonded device clearly showing that the channels have been bonded with minimal deformation.

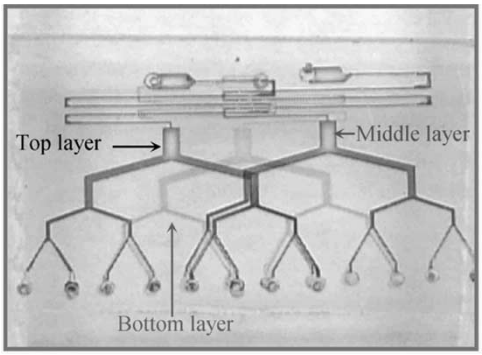

Fig. 10. Microphotograph of three-dimensional microfluidic network using multilayer plastic bonding clearly showing the different layers with microchannel injected with dye.

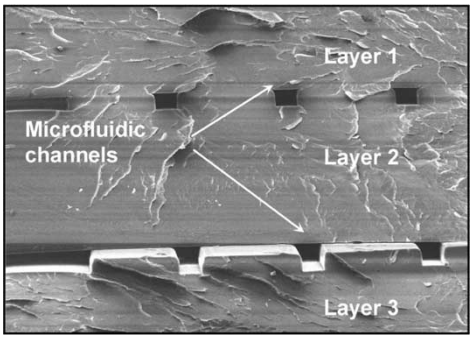

Fig. 11. SEM showing cross-sectional view of multilayer bonded device.

Another factor that could potentially affect the bond strength of the fusion-bonded substrate is the surface condition of the plastic, i.e., whether it is hydrophilic or hydrophobic. Following the plasma modification, as described in the previous section, the substrates were bonded at a temperature of 120 °C and pressure of 10 MPa, to evaluate the effect of the surface modification.

Fig. 12 shows the characterization results of the bond strength as a function the surface contact angle. The debonding force was applied in a normal direction to the bond interface. As Fig. 12 shows, native COC $(\text{contact angle} = 92^\circ)$ has a fairly high bond strength (∼20 MPa) and the bond strength increases as the substrate is made more hydrophilic. This could be due to two reasons: 1) the plasma treatment microscopically roughens the surface thereby increasing the bonding area and 2) the high-energy surface groups can form stronger bonds than the native COC surface groups. Below $\sim 50^\circ$ we see a drop in the bond strength and we hypothesize that the plasma treatment is causing significant damage to the surface creating microcracks on the surface that lead to premature bond failure. On the hydrophobic side, we see a dramatic decrease in bond strength and beyond $\sim 130^\circ$ contact angle there is no bonding between the two substrates.

As noted previously, it is necessary to have a strongly hydrophobic surface for successfully implementing sPROMs-based devices on the COC substrates; however, a strongly hydrophobic surface leads to very weak fusion bond strength. This illustrates the necessity for selective

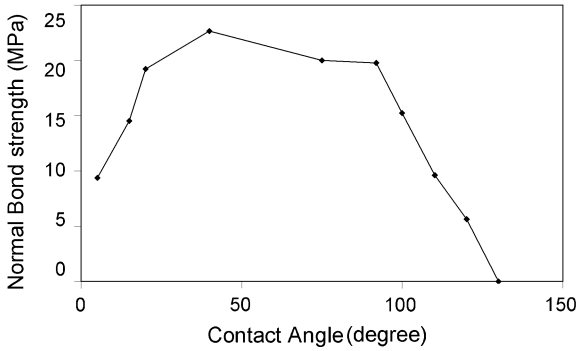

Fig. 12. Effect of variation in contact angle on the bond strength of thermoplastic fusion bonding.

hydrophobic patterning to achieve hydrophobic channel walls where as the remaining substrate is unmodified to ensure high bond strength.

We have successfully characterized the various material properties of COC that are relevant to biochip fabrication including optimizing the injection molding process and a thorough analysis of the surface properties of the COC substrate. These results are of great relevance to the actual biochip fabrication as explained in subsequent sections.

B. Smart Passive Microfluidic Control System

Most biochemical analysis systems require a microfluidic system that is capable of precise control of μL–nL volumes of samples and reagents. The rationale for using passive microfluidic systems has been presented earlier in the introduction. The development of a low-cost, disposable biochip rules out the use of complex and expensive active components such as microvalves or micropumps. This section details the implementation of the structurally programmable microfluidic system, which is *smart passive microfluidic control system* capable achieving the limited microfluidic sequencing steps required in this application. A significant advantage of the sPROMs technology is that it can be used with little or no feedback control system.

The concept of sPROMs as described in this paper can be stated as follows: "*sPROMs is a passive microfluidic control technique where a set of microfluidic manipulations are carried out in a preprogrammed sequence. The microfluidic operations and their sequence is determined primarily by the structural arrangement of the system without the need for an external control signal.*" sPROMs is analogous to the programmable read-only memory (PROM) of a computer where a specified set of instructions is hard-wired into the PROM chip.

1) sPROMs: sPROMs basically consist of a series of microfluidic channels with passive valves located at strategic locations. The passive valve is the flow-regulating unit of the sPROMs system. Fig. 13 shows a microfluidic multiplexer with integrated dispenser that can be used to demonstrate the sPROMs concept [62]–[64].

The microdispenser dispenses a precisely graduated volume of the sampled fluid when dispensing reservoir is

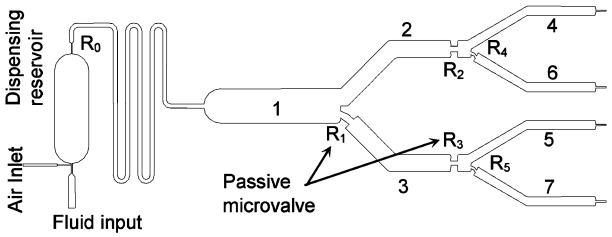

Fig. 13. Microfluidic multiplexer with integrated dispenser used to demonstrate the sPROMs concept.

filled with the liquid and air pressure is applied via the air inlet. The operation of the dispenser is described in more detail in later sections. In the multiplexer, each channel is designed to accommodate the exact same amount of fluid as the succeeding channel pair. At the split-off point, a passive microvalve is placed in one of the channels, to ensure that the fluid will first fill up the other channel. As shown in Fig. 14, fluid will first flow into channel 2 then in channel 3 because of restriction (or passive valve) R_1. The passive microvalve is designed so that after fluid fills up channel 2, the laminar flow pressure drop in that channel exceeds the pressure drop across R_1 and the fluid rushes into channel 3.

Each of these pressures can be calculated theoretically as described in the following section. At the end of each channel pair, there are passive valves (R_2 and R_3) of unequal dimensions, with required flow pressure drops ΔP_{R_2} and ΔP_{R_3}, respectively, that further regulate flow. In this case $\Delta P_{R_2} < \Delta P_{R_3}$, so that fluid first moves past R_2 and fills up channel 4. Now the pressure drops exceed ΔP_{R_3} and fluid rushes into channel 5. By extending this arrangement, fluid can be manipulated to an exact location as desired. In this case, the delivery sequence is 1, 2, 3, 4, etc., as shown clearly in Fig. 14. By changing the locations of the passive valves and/or their relative values with respect to channel size, we can *program* the fluid delivery sequence of the system.

This system works on the principle that the pressure drop across the channels is small compared to the pressure drop across the passive microvalves. This allows the microvalves to serve as primary regulators of the flow sequence.

2) Passive Valve Theory: The passive microvalve is a fundamental building block of the sPROMs system and much research effort has been directed toward the development of efficient passive valves. The passive valve as described in this work is a device that utilizes the surface properties of a *hydrophobic* substrate and a geometrical feature control to regulate fluid flow.

Fig. 15 shows the most basic configuration of the microvalve. When an abrupt change in width is effected across a microchannel fabricated on a hydrophobic substrate, a substantial pressure would be needed to push the fluid across the restriction.

The pressure required to push the fluid into the channel (preceding the passive valve) is expressed by the Hagen-Poiseuille expression for a rectangular channel and can be calculated from (1) [18]

$$\Delta P_1 = \frac{12 L \mu \cdot Q}{w h^3} \tag{1}$$

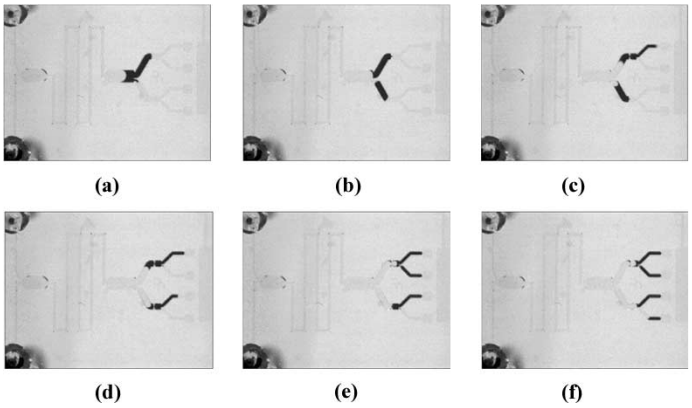

Fig. 14. Operation sequence of the microfluidic multiplexer clearly demonstrating the *smart passive programming* capability of the sPROMs technique.

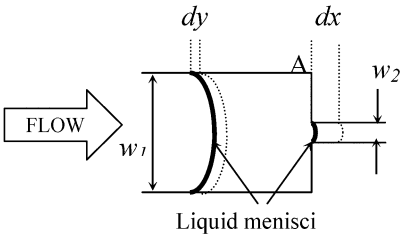

Fig. 15. Abrupt junction passive microvalve.

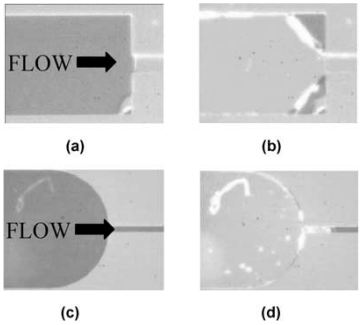

Fig. 16. Flow profiles of passive microvalves. (a) and (b) Abrupt type. (c) and (d) Round type.

where L is the length of the microchannel, μ is the viscosity of the fluid, Q is the flow rate, w is the width, and h is the height of the microchannel.

Once the liquid reaches point A, it encounters an abrupt change in the width of the microchannel. If the fluid is flowing at a very low velocity, such that the surface tension effects are dominant in controlling the flow characteristics, this abrupt change in width results in a significant increase in the pressure required to move the liquid further. The required pressure, to push the liquid into the narrow channel, for this geometry can be derived from the principle of virtual work [32]. Since the fluid entering the narrow channel would experience a higher surface-area-to-volume ratio, there would be an increase in the surface energy of the system. This can be used to derive the expression for pressure needed to overcome the passive valve as

$$\Delta P_2 = 2\sigma_l \cos(\theta_c)\left[\left(\frac{1}{w_1}+\frac{1}{h_1}\right)-\left(\frac{1}{w_2}+\frac{1}{h_2}\right)\right] \quad (2)$$

where w_1, h_1, w_2, and h_2 are width and height of the channels before and after the restriction, respectively, σ_l is the surface tension, and θc is the contact angle of water with the hydrophobic substrate.

For most surface micromachining processes a transition in width is easily achievable whereas variable depth is more difficult to implement. Hence, setting $h_1 = h_2$, (2) is simplified to

$$\Delta P_2 = 2\sigma_l \cos(\theta_c)\left[\frac{1}{w_1}-\frac{1}{w_2}\right]. \quad (3)$$

The passive valve shown in Fig. 15 is not an optimum geometry for the biochip application. When the advancing front reaches the passive valve, it is held there until a high pressure, enough to overcome the passive valve, is applied. The fluid then shoots out of the passive valve at a fairly high velocity. This is expected because once the passive valve is "broken," very little pressure is required to maintain flow through the narrow channel. However, Fig. 16(a) and (b) illustrates the problem with this design. This geometry leads to flow separation at the 90° corners and as a result, a significant amount of fluid is trapped in these corners when the receding front passes through the valve. On the other hand, when a plug of fluid is passed through the geometry shown in Fig. 16(c) and (d), the receding front exits cleanly without leaving behind any evident residue. Thus, it would seem that the abrupt geometry is not well suited for our applications.

As a result we have investigated other geometries that can act as effective passive valves without generating any dead volume.

Fig. 17(a)–(d) shows schematic sketches of the various geometries that can be used as passive valves. Fig. 17(e) shows the simulation results for a constant flow rate (10 μL/min) at the inlet of the passive valves shown in Fig. 17(a)–(d).

As Fig. 17(e) clearly shows, initially there is a slight increase in pressure as the fluid flows up to the passive valve. Then a negative pressure is observed, followed by a large pressure spike indicating that a significant amount of pressure needs to be applied to overcome the passive valve. This clearly demonstrates that all the geometries shown in Fig. 17(a)–(d) can act as effective passive valves [65], [66].

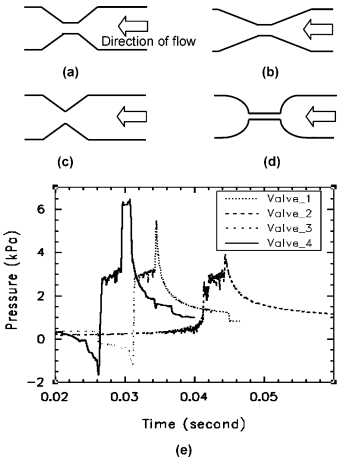

Fig. 17. Passive microvalve geometries. (a) 45° taper type valve. (b) 15° taper type valve. (c) 45° taper valve without restrictor section. (d) Round type valve. (e) Simulated pressure response of above valves at constant flow rate of 10 μL/min.

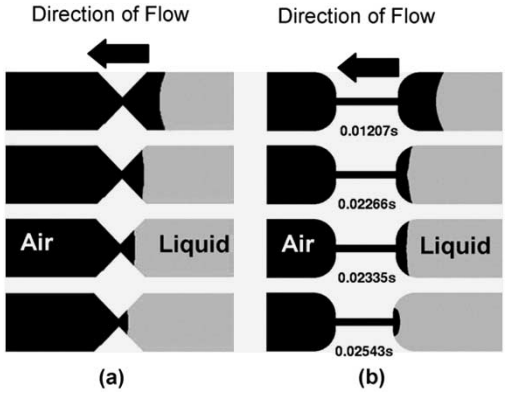

Fig. 18. Pseudohydrophilic effect for: (a) taper type microvalve and (b) round type microvalve.

The simulation results also highlight an interesting aspect of the microvalve structure on a hydrophobic substrate that we describe as the "pseudohydrophilic effect." As shown in Fig. 18, initially the fluid has a convex meniscus (as expected on a hydrophobic substrate) until it reaches the transition region. At this point, in order to maintain the contact angle with the channel wall, the fluid meniscus gets distorted and it changes from convex to straight and then attains a concave shape. The concave shape actually indicates a "hydrophilic" meniscus that will wick the fluid up to the narrow channel. Once the fluid reaches the narrow channel, the meniscus returns to its normal shape and would require the sudden jump in pressure to move it any further. This illustrates the need for a low flow rate system, in which the surface tension forces dominate the flow characteristics.

3) Microdispenser Module: The microdispenser module forms a key microfluidic component of the disposable biochip. The sampled fluid volume is loaded in to the fixed-volume metering microdispenser, which in turn dispenses an exact volume of liquid for further biochemical analysis [65], [66].

Fig. 19 shows a schematic sketch of the microdispenser module. The microdispenser operates on the principle of

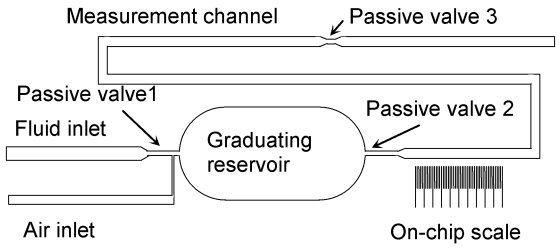

Fig. 19. Schematic sketch of the microdispenser module.

graduated volume measurement where the geometry of the reservoir determines the volume of the microdispenser. The sampled fluid is introduced through the fluid inlet at a low flow rate. The fluid passes through passive valve 1 and the following narrow channel to enter the reservoir. The air inlet is designed to be much smaller than the fluid path between passive valve 1 and the reservoir. This ensures that the fluid does not enter the air inlet. Passive valve 2 at the end of the reservoir prevents the fluid from leaving the reservoir. As long as the applied fluid driving pressure is less than the pressure required to overcome passive valve 2, the fluid will be contained completely within the reservoir.

Then air pressure, higher than the resistance of passive valve 2, is applied via the air inlet line. This causes a split in the liquid column in the narrow section following passive valve 1. At this stage the volume of the fluid contained within the reservoir is isolated within the dispenser. At higher air pressures, the fluid within the reservoir is pushed out toward the right. The fluid is ejected from the reservoir and enters the measurement channel. The measurement channel is designed to accommodate a slightly larger volume than dispensed from the reservoir. Passive valve 3 at the end of the measurement channel stops the ejected fluid from flowing past it unless a higher pressure is applied. An on-chip scale is fabricated in close proximity of the measuring channel to record the position of the rear end of the fluid column. Using the on-chip scale, we can measure the exact length of the fluid column and use that to calculate the dispensed volume.

The device shown in Fig. 19 was implemented initially using rapid prototyping techniques using PDMS fabrication. Fig. 20 shows an actual operation sequence of the microdispenser. Fig. 20(d) shows that the liquid injected is held by passive valve 2 and Fig. 20(e) shows that once air pressure is applied via the air inlet, a split is caused in the liquid column and the fluid is ejected toward the right. Fig. 20(f) shows the dispensed volume is held by passive valve 3, and at this stage the length (and hence volume) can be calculated using the on-chip scale.

We have tested three different dispenser volumes: 50, 100, and 150 nL. The dimension of the on-chip scale allowed for measurements with a resolution of 50 pL. For the designed volumes, this corresponds to less than 0.1% measurement error. The dispensed volume was further verified by an independent mass measurement technique.

Fig. 21 shows the precision measurement results obtained using the on-chip scale. These results are measured for 15 consecutive dispensing cycles for each of the designed dis-

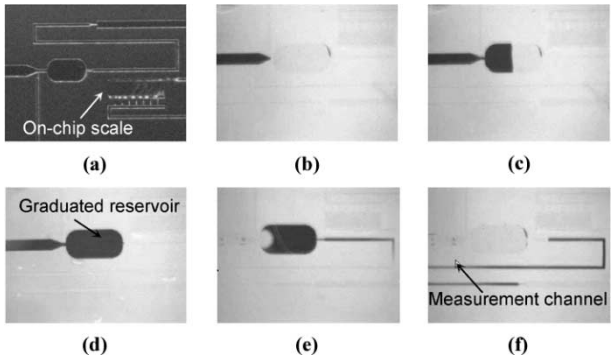

Fig. 20. Microphotographs of microdispenser sequence. (a) Fabricated device. (b) Fluid at reservoir inlet. (c) Reservoir filling. (d) Reservoir filled. (e) Split in liquid column due to air pressure. (f) Fluid ejected to measurement channel and locked in by passive valve.

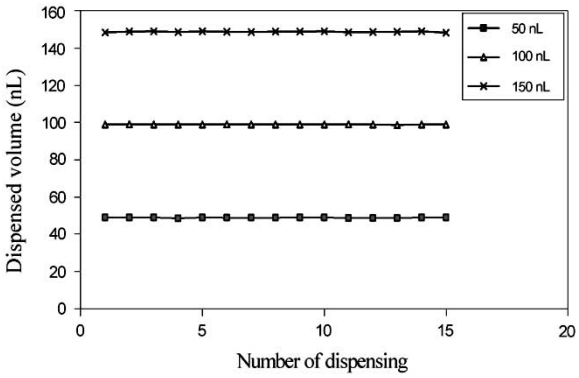

Fig. 21. Precision measurement results for the designed microdispensers.

pensers. As Fig. 21 clearly shows, all three devices have excellent repeatability characteristics. The variation (standard deviation) was 0.3% for the 50-nL dispenser, 0.45% for the 100-nL dispenser, and 0.3% for the 150-nL dispenser.

Fig. 22 shows the long-term performance characteristics of the microdispenser. A set of 25 readings was recorded once every week over a period of six weeks. As shown in Fig. 22, the dispensed volume is very stable over a period of many weeks.

4) Microfluidic Multiplexer With Integrated Dispenser: The microfluidic multiplexer with the integrated dispenser has already been introduced earlier in this paper. Fig. 13 shows a schematic sketch of the implemented multiplexer with integrated microdispenser. As Fig. 13 shows, the design can be thought of as two separate microfluidic devices, the multiplexer and the dispenser, integrated together simply by connecting the outlet of the dispenser to the inlet of the multiplexer.

This highlights an advantage of the sPROMs technique where individual microfluidic devices can be designed and characterized and can also be easily integrated with one another. The addition of the microfluidic multiplexer allows for complex fluid handling where the dispensed volume is divided into four equal volumes and delivered sequentially to each outlet.

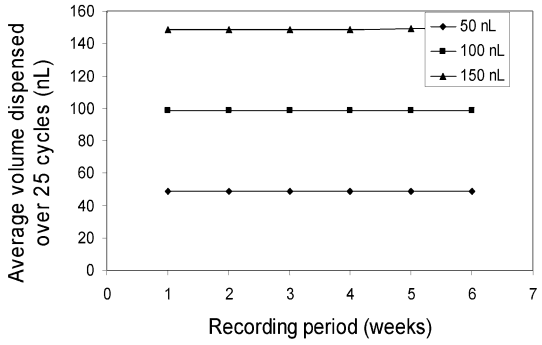

Fig. 22. Long-term reliability measurements.

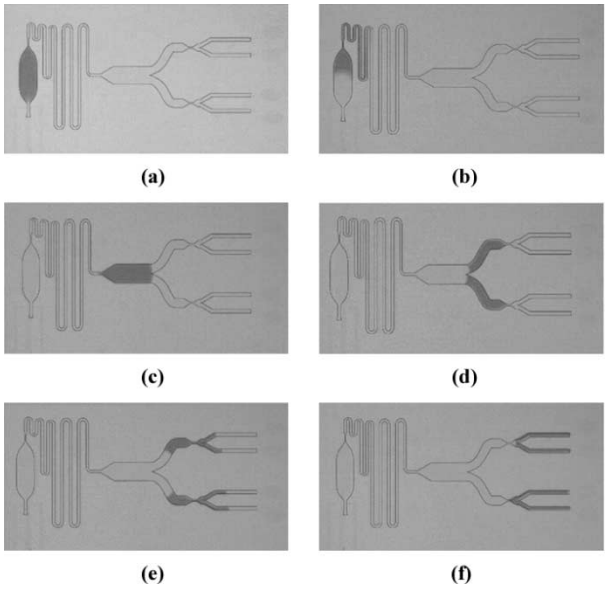

Fig. 23. Microphotographs of fluidic action in a nonsequential multiplexer with the optimized geometry (note: a border has been added for easy visualization).

If the only requirement from the multiplexer is exact fluid division (not necessarily in a sequential fashion) then a much simpler nonsequential multiplexer can also be used. This is accomplished by removing passive valves R_1, R_4, and R_5 in Fig. 13. The design has been optimized to minimize the fluidic residue seen in Fig. 13. The integrated device design was simulated to verify that there was no residue formation. The results of the simulation have also been confirmed experimentally [63].

Fig. 23 shows the actual operation of the nonsequential multiplexer with integrated dispenser. As Fig. 23 clearly shows, the designed dispense volume is successfully ejected without leaving any residues in the dispenser. Furthermore, as the liquid travels down the multiplexer, it is divided equally without any loss in volume.

The multiplexer with integrated dispenser was characterized using the same techniques described in the microdispenser section. The accuracy of the integrated device was characterized at $99.2 \pm 0.1\%$ and the variation between 25 dispensing cycles was less than 0.5% at each outlet.

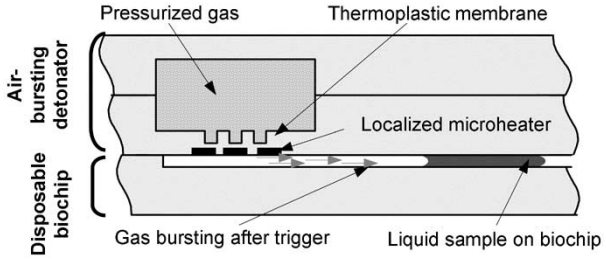

Fig. 24. Schematic drawing of the disposable air-bursting detonator as an alternative on-chip power source.

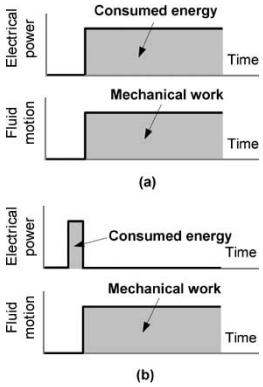

Fig. 25. Consumed electrical power in driving fluids. (a) Conventional micropump. (b) Air-bursting detonator.

C. Air-Bursting Detonators as Alternative On-Chip Power Source

Micropumps are by far the most common microfluidic devices used to produce and control pressure for microfluidic systems. There have been a number of different approaches toward realizing active micropumps with diaphragms, rotary microturbines, and nozzle-diffuser structures using electrostatic, electromagnetic, thermopneumatic, electrohydrodynamic, or magnetohydrodynamic actuations [4]–[9]. However, the active micropumps usually require an on-line electrical power or off-line batteries. For disposable microfluidic biochips or systems the active micropumps should be integrated with disposable batteries. This approach would increase the cost of the biochip and also involves many technical difficulties. So an alternative power source is desirable for the disposable biochips or lab-on-a-chip devices, to power passive-type microfluidic components.

We have developed a novel concept for an alternative on-chip power source to address the problems with the disposable microfluidic biochips and bioanalysis systems. Pressurized gas in a microreservior can be utilized as an energy source to control fluidic sequencing on a disposable biochip. The gas can be compressed and stored for subsequent usage and this pressurized gas can be released upon "triggering" by a short electrical pulse as shown in Fig. 24 [67], [68].

Fig. 24 shows a schematic illustration of the novel disposable air-bursting detonator as an alternative on-chip power source. Pressurized gas, which is compressed and stored in the chamber, produces pressure to drive fluid samples in microchannel upon "triggering" by a so-called detonator (microheater). Once an electric power pulse is sent to the microheater, thermal stress of the membrane will be increased until the membrane is broken (or the thermoplastic membrane will completely melt). After the membrane is broken, the pressurized gas pushes the fluid sample into the microchannel through a broken hole on the membrane. Low power consumption is guaranteed since only one pulsed power is used to burst the pressurized gas.

Fig. 25 can clearly illustrate the advantage of using the air-bursting detonator. In case of a conventional micropump, as shown in Fig. 25(a), a continuous supply of electrical energy must be provided in order to actuate the micropump and cause fluidic displacement. On the other hand, for the air-bursting detonator, the work done in displacing the fluid is accomplished by the potential energy stored in the compressed gas. Only a small energy burst is required to "trigger" the breaking of the membrane to release this stored energy [67].

Initial proof of concept for the air-bursting detonators was demonstrated using a composite silicon/SU8 device. In this case, the SU8 formed a membrane over a through hole etched cavity in a silicon wafer. The silicon wafer was in turn connected to a pressure chamber and the whole assembly could be mounted onto a disposable biochip. Though this device was successful in establishing a proof of concept, it requires complex fabrication and assembly steps, thereby making it of limited use to the disposable biochip application. Hence, a fully microfabricated, plastic-based device has been developed as shown earlier in Fig. 24. The membrane of this device is created by milling/injection molding or embossing a COC plastic wafer. Hence, the pressure-containing reservoir and the thermoplastic membrane are now an integral part of the COC wafer and can be easily assembled to the remaining system.

1) Design and Simulation: In the device shown in Fig. 24, the detonator will have its own "pressure discharge" characteristics due to the gas flow resistance of the hole and the microfluidic channel. The characteristics of this microfluidic "battery" can be easily adjusted by changing the conditions of the microheater having different sizes of the hole, which produces different gas flow resistances and pressure drops.

Dynamic thermomechanical simulation was first conducted by CFD-ACE+ solver module from CFD Research Corporation (CFDRC), Huntsville, AL, to investigate the temperature profile and thermal stress on the microheater and membrane.

Constant material properties (conductivity, resistivity, and specific heat) were reasonably assumed for simulation and the external convection boundary conditions were applied to all boundary surfaces considering heat dissipation by air convection. Fig. 26 shows the thermal profile on the membrane as a function of time.

Fig. 27 shows a ploy of the temperate profile versus time as simulated in the case of Fig. 28. A lower power input has slower response due to heat capacity of the materials and heat

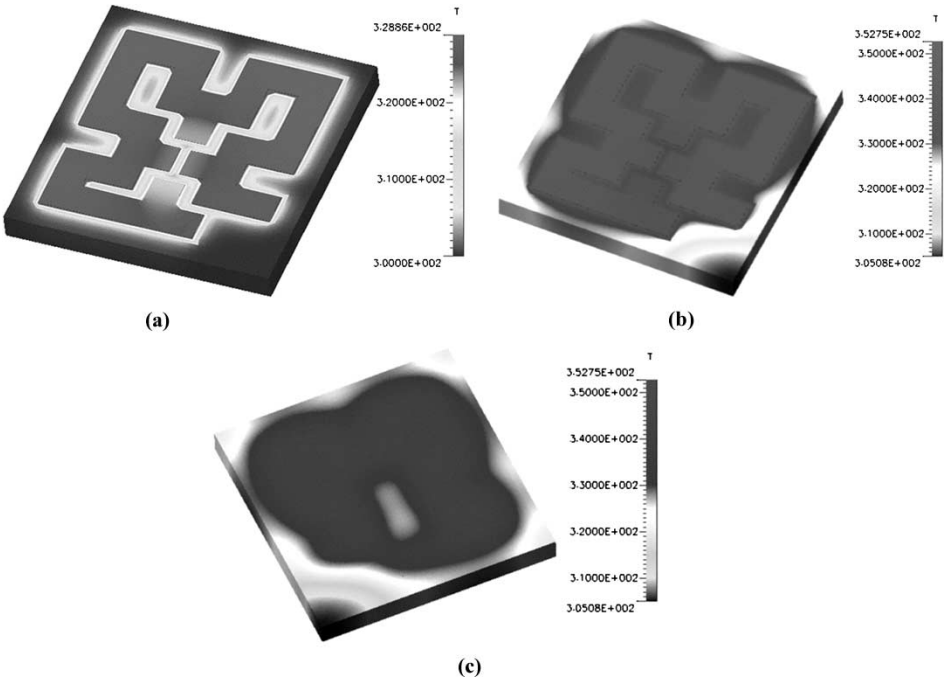

Fig. 26. Dynamic thermomechanical simulation using CFD-ACE+ package. (a) Temperature profile on the top surface at 10 ms. (b) Temperature profile on the top surface at 100 ms. (c) Temperature profile on the bottom surface at 100 ms.

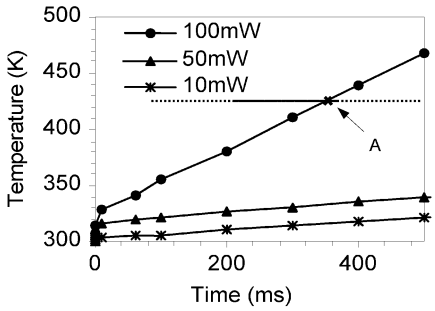

Fig. 27. Dynamic thermomechanical simulation of the heater. Trigger point A is the glass transition temperature of the membrane.

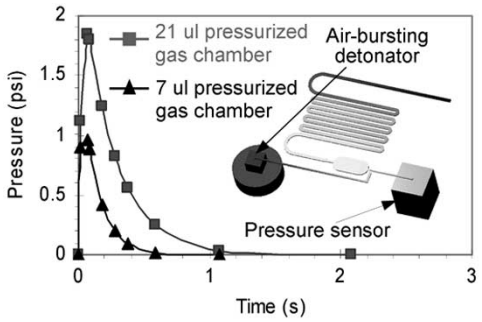

Fig. 28. Dynamic flow simulation of the air-bursting detonator with meander-type long microchannel.

dissipation to air by convection. Pulsed electric current starts to trigger the detonator around 350 ms for the detonator with plastic membrane (the glass transition temperature for the plastic membrane is around 140 °C) with 100 mW of applied power. Dynamic flow simulation was also performed to investigate the flow response when the air-bursting detonator is integrated with meander-type long microchannel as shown in Fig. 28.

2) Fabrication and Experimental Characterization: A variety of different fabrication techniques were explored for the fabrication of the membrane of the air-bursting detonators. We have fabricated the membrane structure using: 1) mechanical machining; 2) injection molding; and 3) embossing techniques. The embossing technique leads to very good membrane structure. For the injection molded and embossed membrane, an annealing step was required to reduce the local buckling on the membrane formed due to thermal stresses during the fabrication process. The microheater pattern was formed by electroplating a nickel pattern onto the membrane structure.

Fig. 29(a) shows a fabricated device. Fig. 29(b) and (c) show the membrane with the heater pattern before and after thermal actuation. The device shown in Fig. 29(a) was coupled to a microfluidic channel to monitor the dynamic pressure response of the air-bursting detonators. Fig. 30 shows the dynamic pressure response of the air-bursting detonators. Comparison with Fig. 28 shows that the response of the air-bursting detonators matches the simulation results closely. As shown in Fig. 30, the addition of a liquid in the microchannel causes an increase in the time as well as magnitude of the peak pressure. The additional time difference can be easily attributed to the delay caused by the liquid motion.

The increase in pressure may seem counterintuitive. When one considers a liquid plug within a microchannel, there exists a finite pressure drop across the advancing and the receding meniscus of the liquid front. The additional pressure

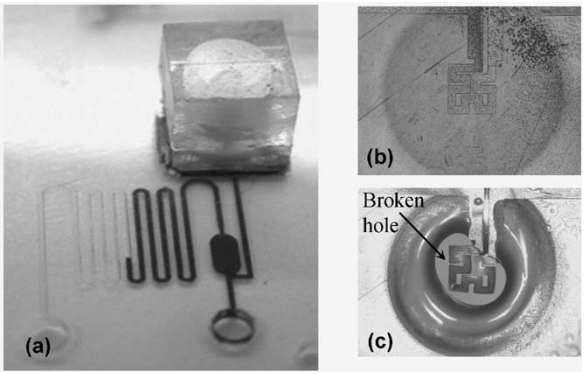

Fig. 29. Fabricated device. (a) Air-bursting detonator integrated with microchannel. (b) The detonator membrane before bursting. (c) The detonator after bursting.

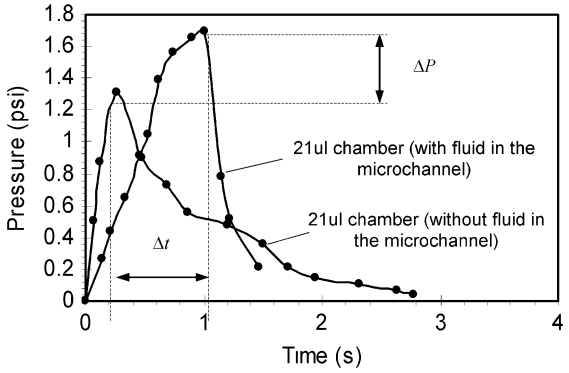

Fig. 30. Dynamic pressure measurement of the air-bursting detonator with serpentine microchannel. With fluid in the microchannel, dynamic pressure drop makes pressure difference (ΔP) and time delay (Δt).

drop seen in Fig. 30 can be attributed to this pressure differential across the liquid meniscus that is superimposed on the pressure delivered by the air-bursting detonator.

III. Diagnostic Functions of the Disposable Biochip

This section presents details about the sampling and the biosensor aspects of the disposable biochip. The biosensors constitute the actual detection mechanism on-chip and are the most significant part of the biochip. The biosensor design has to provide a fast and reliable detection of the analytes and also be compatible with the low-cost, disposable requirements of the biochip.

A. Biosensors

One goal for the biochip development is the development of a fully integrated microbiosensor array for human blood monitoring. Considerable research has already been directed for the fabrication of microbiosensors, which can greatly reduce the sensing cost and make biosensors portable and easy to use. One of the most fundamental sensor designs is the oxygen sensor, which is the basic sensing structure for many other metabolic products such as glucose and lactate. The original concept of an oxygen sensor was proposed by Clark based on an amperometric detection principle [69].

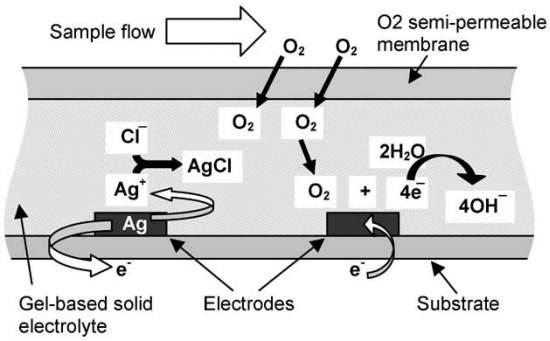

Fig. 31. Electrochemical and analytical principle of the developed biosensor for partial oxygen concentration sensing.

Present-day oxygen sensors are still based on the same principle.

1) Principle of Oxygen, Glucose, and Lactate Sensors: The principle of the oxygen sensor is based on amperometric detection. Fig. 31 shows a schematic representation of an oxygen sensor. When the diffusion profile for oxygen from the sample to electrode surface is saturated a constant oxygen gradient profile is generated. Under these circumstances the detection current is proportional to only to the oxygen concentration in solution.

The gel-based electrolyte is essential for the ion exchange reactions at the anode of the electrochemical pair. The oxygen semipermeable membrane ensures that mainly oxygen molecules permeate through this layer and that the electrochemical cell is not exposed to other ions. A silicone layer was spin-coated and utilized as an oxygen semipermeable membrane because of its high permeability and low signal-to-noise ratio. Water molecules pass through the silicone membrane and reconstitute the gel-based electrolyte so that the Cl^- ions can move near to the anode to coalesce with Ag^+. The number of electrons in this reaction is counted by the measuring system [70].

The electrochemistry for macro scale gives the relationship between current and analyte concentration as

$$\boldsymbol{i} = (nFAD_{\mathrm{O}_2}\Delta[\mathrm{O}_2])/d \tag{4}$$

where $\boldsymbol{i}$ is the signal measured by the amplifying circuit, n is the number of electrons that are exchanged during reaction (four electrons for oxygen sensing), F represents Faraday constant, A represents area of cathode, D_{O_2} is the diffusion constant that varies according to the semipermeable material, $\Delta\,[\mathrm{O}_2]$ represents the difference of oxygen concentration between sample and electrode surface, and d is defined as total thickness of membrane and gel-based electrolyte layer. In actual experiments, D_{O_2} is taken as mean of semipermeable membrane and electrolyte layer. In the saturation case, the oxygen concentration near the electrode surface can be assumed to be zero so that $\Delta\,[\mathrm{O}_2]$ can be directly assumed as oxygen concentration in sample. Using (4), we can calculate the current for different experimental conditions. Such parameters include membrane material, thickness of membrane and solid electrolyte layer, area of electrodes, distance between electrodes, and the shape of electrodes.

The glucose and lactate sensors are an extension of the glucose sensor concept. In a glucose sensor, for example, the glucose molecules are converted to hydrogen peroxide in the presence of glucose oxidase enzyme. This reaction proceeds as follows (in presence of glucose oxidase enzyme):

$$\text{Glucose} \rightarrow \text{Gluconic Acid} + H_2O_2.$$

The hydrogen peroxide molecules from this reaction will subsequently release oxygen that can be detected by an oxygen sensor. The glucose oxidase must be entrapped in a matrix material to prevent enzyme loss during testing. During fabrication, the process temperature has to be limited to ensure that the enzyme will not be denatured. A similar reaction will occur for lactate molecules in the presence of the lactate oxidase enzyme.

When the rate of the enzyme reaction is much larger than glucose/lactate diffusion rate, each molecule that passes through the glucose/lactate semipermeable membrane will be oxidized and generate one hydrogen peroxide molecule, which will be detected by the oxygen sensor as described above.

2) Sensor Fabrication: A significant challenge in developing fully integrated chip-based biosensors is the inability to store liquid electrolytes on-chip. This incompatibility of liquid solution with modern micromachining technology is a big obstacle for disposable and cheap sensing systems. Our approach is to introduce a low melting point solid electrolyte during biosensor fabrication, so that a portable and low-cost detection system is achieved. The electrolyte can be reconstituted just before biochemical detection. This technique is also compatible with mass manufacturing approaches such as spin coating and screen printing allowing us to maintain the low-cost requirement for the disposable biochip.

The fabrication sequence for the biosensor array (oxygen, glucose, and lactate sensors) is described below. One–thousand–angstrom–thick gold was deposited on a 3-in COC wafer with 300-Å-thick titanium as adhesion layer. The gold layer was patterned using positive photoresist-based lithography. Two-micrometer-thick silver was electroplated on the gold patterns to form a gold–silver electrode pair [71].

After patterning the electrodes, the various layers were deposited by spin coating and screen printing. The gel-based electrolyte was heated to 65 °C under continuous stirring. The liquefied electrolyte was spin-coated over the electrode area to achieve a 3-μm-thick electrolyte. The gel-based electrolyte was cured at room temperature. Following this, the semipermeable layer (silicone) was spin coated. This completed the fabrication sequence for the oxygen sensors. To fabricate the glucose and lactate sensors, the glucose (or lactate) oxidase solution was mixed with polyacrylamide in a 4 : 1 ratio and mixed thoroughly. The mixture was then selectively applied over the respective electrodes by screen printing. A polyurethane layer was finally screen printed as glucose/lactate semipermeable membrane. Fig. 32 shows a microphotograph of the fabricated biosensor array with an oxygen, glucose, and lactate sensor. The fabrication sequence is designed such that sensors based on a similar principle and/or fabrication process can be batch processed, thereby reducing the fabrication complexity and the cost of the device.

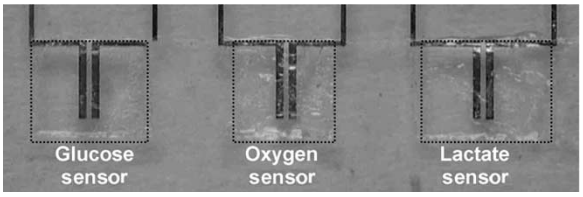

Fig. 32. Microphotograph of the biosensor array showing the different biosensors. Note that a border has been added around the patterned areas for easy visualization.

The materials involved in the biosensor assembly, specifically the solid electrolyte and the enzyme layers, are sensitive to temperature variations. For example, the heat involved in fusion bonding would definitely denature the enzymes and render the sensors useless. Hence, a room temperature UV bonding technique was implemented to assemble the biosensor layer to the fluidic layers.

3) Sensor Characterization: We have investigated numerous parameters to optimize the biosensor design and to evaluate the performance of the biosensors. Among the parameters investigated were the effect of electrode area on sensor performance, dynamic response of the sensor, sensor linearity, and effects of environmental conditions such as temperature on sensor performance.

Fig. 33 shows the linearity characterization results. As Fig. 33 shows, all three developed sensors have fairly linear response characteristics and hence a linear relationship of output current versus concentration can be assumed. This information is crucial to the design of the detection circuit.

Fig. 34 shows the characterization results of the sensor array in terms of the dynamic response and effect of electrode area. Fig. 34(a) shows that the response time of the oxygen sensor is less than a minute, reaching saturation values in $\sim$50 s. The sensor response times are among the fastest reported and can be further improved by optimization of membrane/electrolyte thickness.

The results of Fig. 34(b) are in agreement with (4), which predicts and increased area would lead to higher signals.

IV. Fully Integrated Disposable Biochip Cartridge

A schematic illustration of the multilayer disposable biochip has been presented in the introduction of this paper. The fluidic part of the biochip is based on the structurally programmable microfluidic system presented in Section II-B and the fluid driving system is based on the air-bursting detonators presented in Section II-C. The devices are fabricated using the plastic micromachining techniques described in Section II-A. Finally, the biosensor design is based on the work presented in Section III-A.

Fig. 35 shows the three-dimensional schematic view of the realized biochip with the five-layer architecture. The fabricated chip is only $1\times 1\times 0.25$ in in dimension. The topmost layer has the biosensor patterns, the next two layers constitute the microfluidic control system, and the last two layers are used for the membrane and reservoirs of the air-bursting

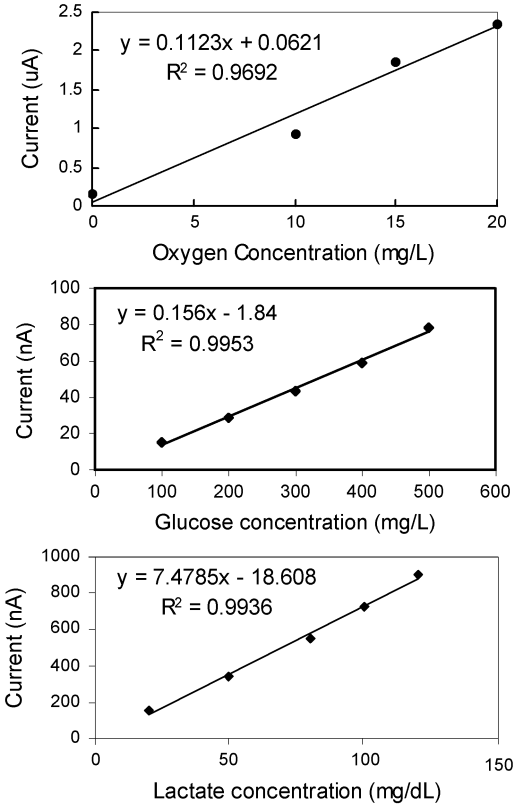

Fig. 33. Linearity characterization results of biosensor array.

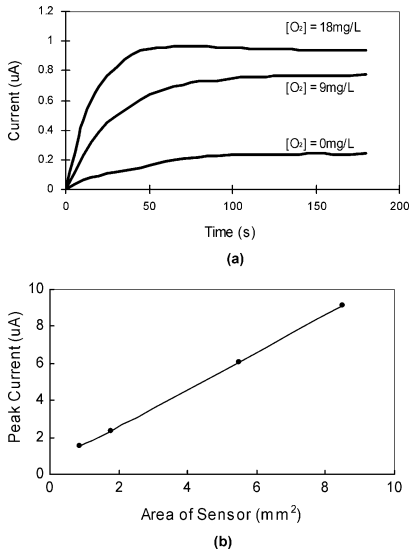

Fig. 34. Characterization results of biosensor. (a) Dynamic response. (b) Effect of electrode area.

detonators. The calibration solution is contained within an on-chip metallic pouch.

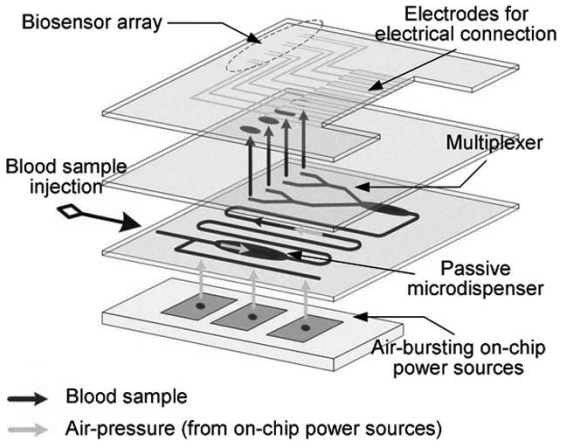

Fig. 35. Schematic illustration of multianalyte detection disposable biochip cartridge. The biochip incorporates on-chip power sources for passive microfluidic manipulation and a biosensor array for blood analysis toward point-of-care systems.

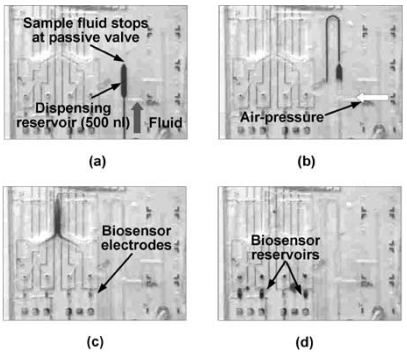

Fig. 36. Microphotographs showing microfluidic operation of disposable biochip. (a) Load sample solution. (b) Fire air-bursting detonators to push sample. (c) Start fluidic multiplexing. (d) Sample solution delivered to sensors.

At the start of the operation sequence, blood sample is loaded via the inlet. The sample will fill up to the microdispenser reservoir. The passive valve at the end of the dispenser prevents further motion of sample. At this stage, air pressure is applied by "detonating" the air-bursting detonators. The liquid then travels down the winding channels, where the eject velocity is reduced and then it enters the multiplexer stage. The multiplexer nonsequentially divides the sample into four equal volumes and each volume is delivered to a biosensor reservoir. The biosensors are mounted on top of this reservoir. When the sample is loaded into the sensor reservoir, the measurement cycle is initiated and the concentrations of the desired analytes are measured.

Fig. 36 shows a sequence of images showing the results of the microfluidic testing of the designed biochip. As shown in Fig. 36(b) when air pressure is applied from the detonator inlet, a split is caused in the sample liquid column and the dispensed volume is pushed out toward the sensor reservoirs. As Fig. 36(c) and (d) clearly show, the liquid is then divided and delivered for sensing. After the detection cycle is completed, the biochip is discarded and a fresh biochip is used for the next test.

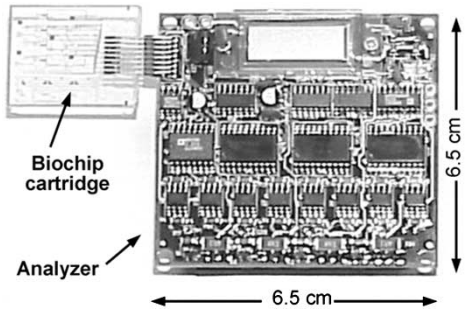

Fig. 37. Biochip cartridge inserted into analyzer module for multiparameter detection.

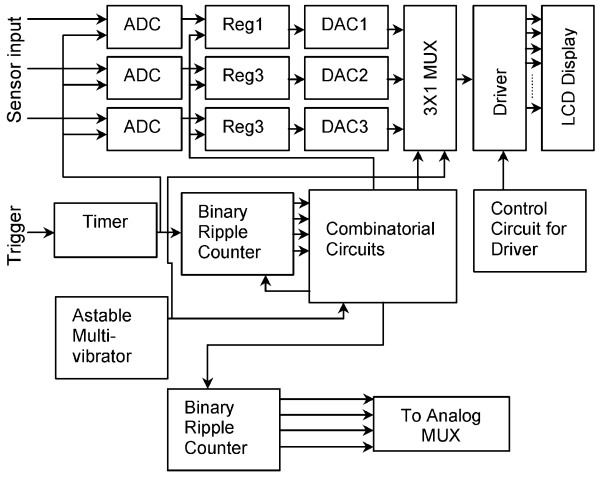

Fig. 38. Block diagram of the detection and display circuit used in the handheld analyzer.

V. Analyzer Module

The disposable biochip is designed is to work with a portable analyzer module that supplies the control signals for the microfluidic sequencing and also has the detection and display units for analyzing the biochemical input.

A. Control and Detection Circuitry

The control and detection circuitry were implemented on a multilayer printed circuit board using surface mount technology (SMT) ICs to minimize the size of the device. The liquid crystal display (LCD) used for displaying the concentration of fluid analytes was a 3.5-digit static duty, elastomer version LCD that met the low power consumption and small size specifications. The overall board dimensions were $2.5\times 2.5\times 1.5$ in, including the batteries. The total power consumption of the board was estimated to be 0.4 W. Fig. 37 shows the SMT board with a biochip mounted in the cartridge holder.

The circuit can be broadly divided into two subsections: the detection and display unit and the pulse driver circuit for providing detonation pulses to the air-bursting detonators.

Fig. 38 shows a block diagram of the detection and display circuit implemented for the biosensor control. The subsystems of this unit are further described below.

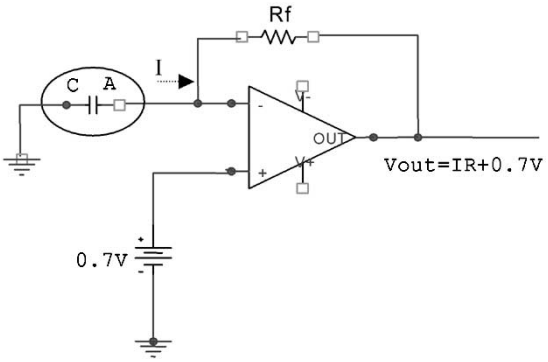

Fig. 39. Simplified view of the detection circuit. The low-offset op-amp is used in a *I–V* converter configuration.

Detection System: The detection system consists of a voltage reference to provide the power supplies to the electrodes in the biosensor and a detection circuit to convert the output signal from the biosensors to a voltage signal. This signal is then amplified; the peak value is detected and displayed.

The power supply to the electrodes needs to be a constant voltage that would not drop below 550 mV, which is required to initiate the electrochemical reaction at the biosensor. Biasing the electrodes to an excess voltage would cause excess thermal dissipation and would disrupt the biosensor performance. When a bias signal is provided to the anode, the reaction starts and current from the electrodes rises linearly and saturates to a peak value in the range of 100 nA–20 μA (depending on the type of sensor). An operational amplifier with a very low offset voltage was used in a current to voltage (*I–V*) converter configuration to amplify the current signal to an equivalent voltage signal as shown in Fig. 39.

Control Logic Circuitry: The control logic circuit is basically an analog to digital converter that converts the peak value of the output signal from the detection system into a digital value. The sampling interval is adjusted such that the analog value is acquired when the biosensor signal has saturated at its peak value. This value is stored in an eight-bit register. The output signals for each of the three sensors are sequentially multiplexed using a 3×1 analog multiplexer. Each input channel is selected by external control signals and is directed to the display where the data is displayed after being reconverted to an analog format. The display is conducted in a cyclic fashion, where one analyte concentration is displayed at a time in a sequential fashion.

Display Driver Circuitry: This is an interface between the detection/control logic circuitry and the LCD display. A display driver is required to generate appropriate frontplane and backplane waveforms and, hence, switch on the corresponding segments so that the analog value is displayed on the LCD. A square wave is supplied to the backplane electrodes of the LCD display and to the driver IC. The driver IC modifies the phase input depending on the input data.

Pulse Driver Circuit: The driver circuit is designed to sequentially "detonate" multiple membranes with a fixed time delay where each membrane detonation requires a 280-mA current pulse for 800-ms duration.

A set of delay elements is constructed using monostable multivibrators with 555 timers. A start pulse is applied to the first timer, which introduces a delay of 2.5 s and activates the driver element. The start pulse is also propagated to the next timer element and after a further delay of 2.5 s, the second driver element is activated. A total of four delay timers and driver elements have been implemented on the SMT boards allowing for sequential control over four air-bursting detonators. The duration of the delay timers is externally adjustable. The driver element is a Darlington pair configuration of bipolar junction transistors to supply a constant current to the detonator heaters. The designed Darlington pair driver element can provide a continuous current of up to 2 A if required and is more than sufficient to provide the specified current pulse for the air-bursting detonators.

The designed SMT boards have been fully tested and characterized. Extensive biosensor testing has been conducted using the developed SMT boards.

B. ASIC Design and Testing

Scaling the SMT components onto application-specific IC (ASIC) chips can significantly reduce the size of the electronic system. With this goal, we have designed and tested two ASIC chips:

Analog ASIC: consisting of *I–V* circuits for electrochemical detection, voltage reference, comparator circuitry, and compensation circuitry for the op-amp.

Mixed-Signal ASIC: consisting of analog-to-digital converter, digital-to-analog converter, Clock Generator, and the Control Circuitry for the display driver.

The designed ASIC chips (single channel) were successfully tested to obtain a reliable signal from the biosensors. We are currently developing advanced versions of the ASIC design that are capable of acquiring data from a biosensor array. The second-generation ASIC chips would also have the delay control elements for the detonator activation. The start signal from the ASIC chips would then be amplified by using discrete power components and the resultant current pulse can be used to melt the detonator membrane.

C. Point-of-Care Testing for Clinical Diagnostics

The disposable biochip developed in this work was tested with the developed SMT electronics system described in the previous sections. The actual testing with blood samples was conducted at Ohio State University Medical Center, Columbus. The results of the testing are presented in this section.

Fig. 40 shows the test results of the biosensor array with whole blood for glucose and lactate measurement. The results clearly indicate that our sensor array has a very linear response in the normal detection limits for both glucose and lactate. The normal physiological limits (daily average) for glucose are 90–120 mg/dL. The glucose sensors developed in this work can detect glucose concentrations from 50–250 mg/dL and the lactate sensor has been successfully tested for 2–12 mg/dL. These results clearly prove the utility of the developed biosensor array and the disposable biochip for clinical diagnostic applications.

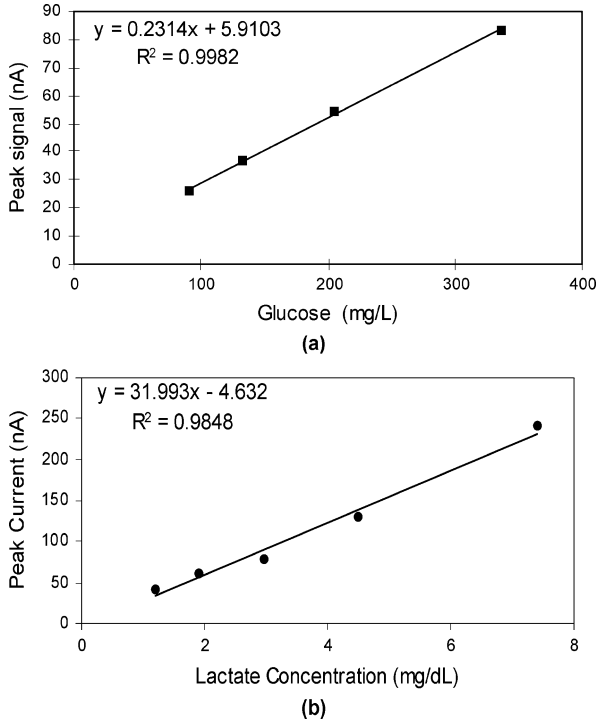

Fig. 40. Measurements results from *actual human blood* samples. (a) Glucose sensor. (b) Lactate sensor.

VI. Conclusion

This paper provides a comprehensive review of the development of a smart, disposable lab-on-a-chip device for biochemical detection of parameters such as blood gas concentration and glucose and lactate concentrations. A number of significant breakthroughs have been accomplished as a part of this work. Notably, the development of a smart passive microfluidic control system that is ideally suited for miniature biochemical analysis systems. We have also developed a novel alternative power source by using the stored potential energy of a compressed gas on a microscale for fluidic driving applications. The biosensor arrays developed in this work are well suited to mass production approach and have been optimized toward accurate and fast measurements. We also developed and characterized novel plastic micromachining processes to implement the low-cost, disposable biochip. The fully integrated biochip developed in this work is only $1 \times 1 \times 0.25$ in in dimensions and incorporates all the functionality required for testing clinically relevant parameters from human blood. Furthermore, the analyzer developed in this work is of immediate relevance to portable biochemical detection applications. We believe the results of this work can have a significant impact toward the development of rapid and affordable point-of-care testing systems.

References

[1] E. Vespoorte, "Microfluidic chips for clinical and forensic analysis," *Electrophoresis*, vol. 23, pp. 677–712, 2002.

[2] R. Ehrnstrom, "Miniaturization and integration: Challenges and breakthroughs in microfluidics," *Lab. Chip*, vol. 2, pp. 26N–30N, 2002.

[3] R. Service, "Lab. on a chip: Coming soon: The pocket DNA sequencer," *Science*, vol. 282, no. 5338, pp. 399–401, 1998.

[4] F. Vinet, P. Chaton, and Y. Fouillet, "Microarrays and microfluidic devices: Miniaturized systems for biological analysis," *Microelectron. Eng.*, vol. 61–62, pp. 41–47, 2002.
[5] C. Malins, M. Niggemann, and B.D. MacCraith, "Multi-analyte optical chemical sensor employing a plastic substrate," *Measure. Sci. Tech.*, vol. 11, no. 8, pp. 1105–1110, Aug. 1, 2000.
[6] P. Bergstrom, K. Wise, S. Patel, and J. Schwank, "A micromachined surface work-function gas sensor for low-pressure oxygen detection," *Sens. Actuators B*, vol. 42, no. 3, pp. 195–204, Aug. 1997.
[7] L. Cao, S. Mantell, and D. Polla, "Design and simulation of an implantable medical drug delivery system using microelectromechanical systems technology," *Sens. Actuators*, vol. A 94, pp. 117–125, 2001.
[8] M. Burns, B. Johnson, S. Brahmasandra, K. Handique, J. Webster, M. Krishnan, T. Sammarco, P. Man, D. Jones, D. Heldsinger, C. Mastrangelo, and D. Burke, "An integrated nanoliter DNA analysis device," *Science*, vol. 282, pp. 484–487, 1998.
[9] P. Grodzinski, R. Liu, B. Chen, J. Blackwell, Y. Liu, D. Rhine, T. Smekal, D. Rhine, T. Smekal, D. Ganser, C. Romero, H. Yu, T. Chan, and N. Kroutchinina, "Development of plastic microfluidic devices for sample preparation," *Biomed. Microdev.*, vol. 3, no. 4, pp. 275–283, 2001.
[10] T. Dinh, G. Griffin, D. Stokes, and A. Wintenberg, "Multi-functional biochip for medical diagnostics and pathogen detection," *Sens. Actuators B*, vol. 90, pp. 104–111, 2003.
[11] L. Kricka, "Microchips, microarrays, biochips, and nanochips: Personal laboratories for the 21st century," *Clin. Chim. Acta*, vol. 307, pp. 219–223, 2001.
[12] I. Lauks, "Microfabricated biosensors and microanalytical systems for blood analysis," *Acc. Chem. Res.*, vol. 31, pp. 317–324, 1998.
[13] J. Ko *et al.*, "A polymer-based microfluidic device for immunosensing biochips," *Lab. Chip*, vol. 3, pp. 106–113, 2003.
[14] T. Dinh and B. Cullum, "Biosensors and biochips: Advances in biological and medical diagnostics," *Fresenius J. Anal. Chem.*, vol. 366, pp. 540–551, 2000.
[15] M. Freemantle, "Downsizing chemistry," *Chem. & Eng. News*, pp. 27–36, Feb. 22, 1999.
[16] D. Figeys and D. Pinto, "Lab-on-a-chip: A revolution in biological and medical sciences," *Anal. Chem.*, vol. 72, pp. 330–335, 2000.
[17] S. Shoji and M. Esashi, "Microflow device and systems," *J. Micromech. Microeng.*, vol. 4, pp. 157–171, 1994.
[18] G. Kovacs, *Micromachined Transducers Sourcebook*. New York: WCB-McGraw Hill, 1998.
[19] W. Schomburg, J. Fahrenberg, D. Maas, and R. Rapp, "Active valves and pumps for microfluidcs," *J. Micromech. Microeng.*, vol. 3, pp. 216–218, 1993.
[20] C. H. Ahn, T. Henderson, W. Heineman, and B. Halsall, "Development of a generic microfluidic system for electrochemical immunoassay-based remote bio/chemical sensors," in *Proc. μ TAS'98 Workshop*, pp. 225–230.
[21] D. Sadler, K. Oh, C. Ahn, S. Bhansali, and H. T. Henderson, "A new magnetically actuated microvalve for liquid and gas control applications," in *Proc. Transducers'99*, pp. 1812–1815.
[22] M. Hirano, K. Yanagisawa, H. Kuwano, and S. Nakano, "Microvalve with ultra-low leakage," in *Proc. 10th Int. Workshop MEMS '97*, pp. 323–326.
[23] M. Koch, N. Harris, A. Evans, N. White, and A. Brunnschweiler, "A novel micropump design with thick-film piezoelectric actuation," *Measure. Sci. Technol.*, vol. 8, pp. 49–57, 1997.
[24] H. Chou, M. Unger, and S. Quake, "A microfabricated rotary pump," *Biomed. Microdev.*, vol. 3, no. 4, pp. 323–330, 2001.
[25] S. Zeng, C. Chen, J. Mikkelsen, and J. Santiago, "Fabrication and characterization of electroosmotic micropumps," *Sens. Actuators*, vol. B 79, pp. 107–114, 2001.
[26] G. Fuhr, T. Schnelle, and B. Wagner, "Travelling wave driven microfabricated electrohydrodynamic pumps for liquids," *J. Micromech. Microeng.*, vol. 4, pp. 217–226, 1994.
[27] A. Lemoff and A. Lee, "An AC magnetohydrodynamic micropump," *Sens. Actuators*, vol. B 63, pp. 178–185, 2000.
[28] W. Schomburg and B. Scherrer, "3.5 mm thin valves in titanium membranes," *J. Micromech. Microeng.*, vol. 2, pp. 184–186, 1992.
[29] A. Terray, J. Oakey, and D. Marr, "Fabrication of colloidal structures for microfluidic applications," *Appl. Phys. Lett.*, vol. 81, no. 9, pp. 1555–1557, 2002.
[30] Q. Yu, J. Bauer, J. Moore, and D. Beebe, "Responsive biomimetic hydrogel valve for microfluidics," *Appl. Phys. Lett.*, vol. 78, no. 17, pp. 2589–2591, 2001.
[31] N. Jeon, D. Chiu, C. Wargo, H. Wu, I. Choi, J. Anderson, and G. Whitesides, "Design and fabrication of integrated passive valves and pumps for flexible polymer 3-dimensional microfluidic systems," *Biomed. Microdev.*, vol. 4, no. 2, pp. 117–121, 2002.
[32] K. Hosokawa, T. Fujii, and I. Endo, "Droplet-based nano/picoliter mixer using hydrophobic microcapillary vent," *Proc. 12th IEEE Int. Conf. MEMS '99*, pp. 388–393.
[33] K. Handique, B. Gogoi, D. Burke, and C. Mastrangelo, "Microfluidic flow control using selective hydrophobic patterning," in *Proc. Micromachined Devices and Components*, vol. 3224, 1999, pp. 210–220.
[34] M. McNeely, M. Spute, N. Tusneem, and A. Oliphant, "Hydrophobic microfluidics," in *Proc. Microfluidic Devices and Systems*, vol. 3877, 1999, pp. 210–220.
[35] M. Madou, Y. Lu, S. Lai, and S. Daunert, "A centrifugal microfluidic platform—A comparison," in *Proc. μ TAS 2000 Conf.*, pp. 565–570.
[36] R. Miyake, T. Lammerink, M. Elwenspoek, and J. Fluitman, "Micromixer with fast diffusion," in *Proc. MEMS'93*, pp. 248–253.
[37] D. Beebe, R. Adrian, M. Olsen, M. Stremler, H. Aref, and B. Jo, "Passive mixing in microchannels: Fabrication and flow experiments," *Mecanique Ind.*, vol. 2, no. 4, pp. 343–348, July–Aug. 2001.
[38] S. Bohm, K. Greiner, S. Schlautmann, S. Vries, and A. Berg, "A rapid-vortex micromixer for studying high-speed chemical reactions," presented at the UTAS 01, Monterey, CA, 2001.
[39] A. Stroock, S. Dertinger, A. Ajdari, I. Mezic, H. Stone, and G. Whitesides, "Chaotic mixer for microchannels," *Science*, vol. 295, pp. 647–651, 2002.
[40] C.-C. Hong, J.-W. Choi, and C. H. Ahn, "A novel in-plane passive micromixer using Coanda effect," in *Proc. 5th Int. Conf. Micro Total Analysis Systems 2001*, pp. 31–33.
[41] J. Brody and P. Yager, "Diffusion-based extraction in a microfabricated device," *Sens. Actuators A*, vol. 54, no. 1–3, pp. 704–708, 1996.
[42] B. Weigl and P. Yager, "Microfluidic diffusion-based separation and detection," *Science*, vol. 283, pp. 346–347, 1999.
[43] T. Desai, D. Hansford, and M. Ferrrari, "Micromachined interfaces: New approaches in cell immunoisolation and bimolecular separation," *Biomol. Eng.*, vol. 17, no. 1, pp. 23–36, 2000.
[44] F. Martin and C. Grove, "Microfabricated drug delivery systems: Concepts to improve clinical benefit," *Biomed. Microdev.*, vol. 3, no. 2, pp. 97–108, 2001.
[45] T. Nagakura, K. Ishihara, T. Furukawa, K. Masuda, and T. Tsuda, "Auto-regulated osmotic pump for insulin therapy by sensing glucose concentration without energy supply," *Sens. Actuators B*, vol. 34, no. 1–3, pp. 229–233, 1996.
[46] Y. Su, L. Lin, and A. Pisano, "Water-powered, osmotic microactuator," in *Proc. IEEE MEMS 2001*, pp. 393–396.
[47] G. Walker and D. Beebe, "A passive pumping method for microfluidic devices," *Lab. Chip*, vol. 2, pp. 131–134, 2002.
[48] J. McDonald, D. Duffy, J. Anderson, D. Chiu, H. Wu, O. Schueller, and G. Whitesides, "Fabrication of microfluidic systems in poly(dimethylsiloxane)," *Electrophoresis*, vol. 21, no. 1, pp. 27–40, Jan. 2000. no. 1.
[49] T. Fujii, "PDMS—Based microfluidic devices for biomedical applications," *Microelectron. Eng.*, vol. 61–62, pp. 907–914, 2002.
[50] L. Lee, M. Madou, K. Koelling, S. Daunert, S. Lai, C. Koh, Y. Juang, Y. Lu, and L. Yu, "Design and fabrication of CD-like microfluidic platforms for diagnostics: Polymer-based microfabrication," *Biomed. Microdev.*, vol. 3, no. 4, pp. 339–351, 2001.
[51] H. Becker and C. Gartner, "Polymer microfabrication methods for microfluidic analytical applications," *Electrophoresis*, vol. 21, pp. 12–26, 2000.
[52] H. Becker and L. Locascio, "Polymer microfluidic devices," *Talanta*, vol. 56, pp. 267–287, 2002.
[53] K. Sugita, "Application of photodegradable polymers to imaging and microfabrication technologies: A review of recent research papers in the last 4 years," *Prog. Org. Coatings*, vol. 31, pp. 87–95, 1997.
[54] H. Becke and W. Dietz, "Microfluidic devices for μ TAS applications fabricated by polymer hot embossing," in *Proc. SPIE Conf. Microfluidic Devices*, 1998, pp. 177–182.
[55] S. Metz, R. Holzer, and P. Renaud, "Polyimide-based microfluidic devices," *Lab. Chip*, vol. 1, pp. 29–34, 2001.
[56] Z. Wu, N. Xanthopoulos, F. Reymond, J. Rossier, and H. Girault, "Polymer microchips bonded by oxygen-plasma activation," *Electrophoresis*, vol. 23, pp. 782–790, 2002.

[57] Y. Wang and M. Ferrari, "Surface modification of micromachined silicon filters," *J. Mater. Sci.*, vol. 35, pp. 4923–4930, 2000.
[58] J.-W. Choi, S. Kim, R. Trichur, H. J. Cho, A. Puntambekar, R. L. Cole, J. R. Simkins, S. Murugesan, K. S. Kim, J.-B. Lee, G. Beaucage, J. H. Nevin, and C. H. Ahn, "A plastic micro injection molding technique using replaceable mold-disks for disposable microfluidic systems and biochips," in *Proc. 5th Int. Conf. Micro Total Analysis Systems 2001*, pp. 411–412.
[59] R. Trichur, S. Kim, X. Zhu, J. W. Suk, C.-C. Hong, J.-W. Choi, and C. H. Ahn, "Development of plastic microneedles for transdermal interfacing using injection molding techniques," in *Proc. 6th Int. Conf. Micro Total Analysis Systems 2002*, pp. 395–397.
[60] S. Kim, R. Trichur, G. Beaucage, C. H. Ahn, and B. H. Kim, "New plastic microinjection molding technique for extremely tall plastic structures using remote infrared radiation heating method," in *Proc. 10th Solid-State Sensor, Actuator and Microsystems Workshop*, 2002, pp. 206–209.
[61] A. Puntambekar, S. Murugesan, R. Trichur, H. Cho, S. Kim, J. W. Choi, and C. H. Ahn, "Effect of surface modification on thermoplastic fusion bonding for 3-D microfluidics," in *Proc. μTAS 2002*, pp. 425–427.
[62] C. Ahn, A. Puntambekar, S. M. Lee, H. C. Cho, and C. C. Hong, "Structurally programmable microfluidic systems," in *Proc. μ TAS 2000*, pp. 205–208.
[63] A. Puntambekar, J.-W. Choi, C. H. Ahn, S. Kim, S. Bayyuk, and V. B. Makhijani, "An air-driven fluidic multiplexer integrated with microdispensers," in *Proc. 5th Int. Conf. Micro Total Analysis Systems 2001*, pp. 78–80.
[64] A. Puntambekar, S. Lee, H. J. Cho, and C. H. Ahn, "On-chip microfluidic multiplexers for biochemical reactor and mixers," presented at the IEEE World Congr. Biomedical Physics, Chicago, IL, 2000.
[65] A. Puntambekar, H. J. Cho, C.-C. Hong, J.-W. Choi, C. H. Ahn, S. Kim, and V. B. Makhijani, "A new fixed-volume metering microdispenser module based on sPROM's technology," in *Tech. Dig. 11th Int. Conf. Solid-State Sensors and Actuators*, 2001, pp. 1240–1243.
[66] A. Puntambekar, J.-W. Choi, C. H. Ahn, S. Kim, and V. B. Makhijani, "Fixed-volume metering microdispenser module," *Lab. Chip*, vol. 2, no. 4, pp. 213–218, 2002.
[67] C.-C. Hong, J.-W. Choi, and C. H. Ahn, "Disposable air-bursting detonator as an alternative on-chip power source," in *Proc. 15th IEEE MEMS Workshop (MEMS'02)*, Las Vegas, NV, Jan. 20–24, 2002, pp. 240–243.
[68] ——, "A disposable on-chip air detonator for driving fluids on point-of-care systems," in *Proc. 6th Int. Conf.Micro Total Analysis Systems 2002*, pp. 949–951.
[69] L. C. Clark Jr., "Monitor and control of blood and tissue oxygen tensions," *Trans. Amer. Soc. Artif. Internal Organs*, vol. 2, pp. 41–49, 1956.
[70] C. Gao, J.-W. Choi, M. Dutta, S. Chilukuru, J. H. Nevin, J. Y. Lee, M. G. Bissell, and C. H. Ahn, "A fully integrated biosensor array for measurement of metabolic parameters in human blood," in *Proc. 2nd Annu. Int. IEEE-EMBS Special Topic Conf. Microtechnologies in Medicine and Biology*, 2002, pp. 223–226.
[71] C. Gao, J.-W. Choi, and C. H. Ahn, "A novel glucose biosensor with gel-based solid electrolyte and microheater structure for rapid detection," in *Proc. 7th World Congr. Biosensors*, 2002, pp. 2–3.68.

Chong H. Ahn received the Ph.D. degree in electrical and computer engineering from the Georgia Institute of Technology, Atlanta, in 1993.

From 1993 to 1994, he was a Postdoctoral Associate at the Georgia Institute of Technology and at IBM T. J. Watson Research Center, Yorktown Heights, NY. In 1994, he joined the Department of Electrical and Computer Engineering and Computer Science at the University of Cincinnati, Cincinnati, OH, as an Assistant Professor, where he currently holds the rank of Professor in the Departments of Electrical Engineering and Biomedical Engineering. He is also the Director of the Microsystems and BioMEMS Lab at the University of Cincinnati. He has published approximately 170 journal and conference proceeding papers related to the MEMS, bioMEMS, Microfluidics, and lab-on-a-chip areas, including numerous invited talks from the international conferences, and holds four U.S. patents. He is currently a member of the Editorial Board of the *Journal of Micromechanics and Microengineering*. His research interests include all aspects of design, fabrication, and characterization of magnetic sensors, magnetic MEMS devices, microfluidic devices and systems, BioMEMS devices, plastic-based disposable biochips, point-care blood analyzers, portable biochemical detection systems, protein chips, lab on a chips, and biophotonics and MEMS devices.

Dr. Ahn heads the Cincinnati Chapter of the Electrochemical Society (ECS). He organized several international conferences related to magnetic MEMS and BioMEMS as CoChairs and Organizers, including the Microfluidic Devices and Systems Conference ('98, '99) in SPIE and the International Symposium on Magnetic Materials, Processes and Devices (1998, 2000) for the ECS. In addition, he served the program committee for numerous international conferences related to microsensors, bioMEMS and MEMS, including the IEEE MEMS Conference. He is an Associate Editor of the IEEE SENSORS JOURNAL.

Jin-Woo Choi received the B.S. and M.S. degrees in electrical engineering from Seoul National University, Seoul, Korea, in 1994 and 1996, respectively, and the Ph.D. degree in electrical engineering from the University of Cincinnati, Cincinnati, OH, in 2001.

He was a Research Assistant Professor at the University of Cincinnati, where he participated in the development of plastic lab on a chip for blood analysis. He is currently an Assistant Professor in the Department of Electrical and Computer Engineering at Louisiana State University, Baton Rouge. His research interests include magnetic particle separators, micromixers, microfluidic systems for biochemical detection, micro total analysis systems (μ-TAS), lab on a chip, bioelectronics, and bioMEMS components and systems for biological applications.

Gregory Beaucage received the B.S. degree in zoology and chemical engineering from the University of Rhode Island, Kingston, and the Ph.D. degree in polymer science and engineering from the University of Massachusetts, Amherst, in 1991.

He served as a Patent Examiner reviewing biomedical material patents for four years after his BS degree. From 1991 to 1994, he was a Postdoc and Research Scientist at Sandia National Laboratories, Albuquerque, NM, conducting research on high-performance polymers and ceramics. Since 1994, he has been a faculty member in Chemical and Materials Engineering at the University of Cincinnati, Cincinnati, OH. He has over 70 peer-reviewed publications in the field of polymer and materials science and has edited one book. His current research interests include polymer processing and physics, synthesis of nanostructured ceramics for applications such as polymer reinforcement, and materials for MEMS applications.

Prof. Beaucage is a member of the American Chemical Society, American Physical Society, Polymers Division, American Institute of Chemical Engineers, and the Materials Research Society.

Joseph H. Nevin (Member, IEEE) received the B.S.E.E., M.S., and Ph.D. degrees in electrical engineering from the University of Cincinnati, Cincinnati, OH, in 1964, 1966, and 1974, respectively.

From 1960 through 1964, he was employed part-time with RCA as a circuit design engineer. In 1967, he joined the Department of Electrical and Computer Engineering and Computer Science at the University of Cincinnati, where he is now a Professor. He also currently serves in an administrative role in the College of Engineering as Assistant Dean for Freshman Engineering. Part of his research thrust in the past has been directed toward the study of electronic materials used in integrated circuit fabrication. Central to much of that work was the characterization of polymer materials used as dielectrics. In particular, research on polyimide has disclosed some of the fundamentals of the conduction mechanisms responsible for dielectric leakage currents. Later work with the use of polyimide has resulted in the development of a practical humidity sensor by using the slight tendency for polyimide to absorb moisture. Pressure, humidity, and chemical sensors have been fabricated as a part of this research program. His work in analog circuit design has included switched capacitor filters and design methodologies for folded-cascode amplifiers. Basic design work was done on behavioral modeling of circuits using neural networks. Current research activity is directed toward the development of analog circuits necessary for signal processing in conjunction with MEMS-based sensors as a part of a team effort to design systems for blood biochemical detection.

Dr. Nevin is a Member of the American Society for Engineering Education, Tau Beta Pi, and Eta Kappa Nu, in addition to being a Registered Professional Engineer in the State of Ohio. He is the recipient of numerous teaching awards.

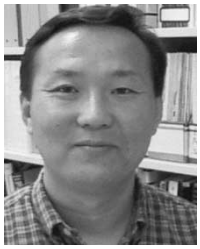

Jeong-Bong Lee received the B.S. degree in electronics engineering from Hanyang University, Seoul, Korea, in 1986 and the M.S. and Ph.D. degrees in electrical engineering from the Georgia Institute of Technology (Georgia Tech), Atlanta, in 1993 and 1997, respectively.

From 1997 to 1999, he was a Research Engineer at Georgia Tech. From 1999 to 2001, he was an Assistant Professor at Louisiana State University, Baton Rouge. Since 2001, he has been an Assistant Professor in the Department of Electrical Engineering, University of Texas at Dallas, Richardson. His current research interests are in the areas of RF/microwave MEMS, MEMS packaging technique, nanophotonic devices, micro/nano assemblers, and chemical/biological sensors.

Dr. Lee is a recipient of the National Science Foundation's Faculty Early Career Development Award.

Aniruddha P. Puntambekar received the B.S. degree in electrical engineering, from the University of Pune, Pune, India, in 1996 and the M.S. degree in biomedical engineering from the University of Toledo, Toledo, OH, in 1998. He is currently working toward the Ph.D. degree in the Microsystems and BioMEMS lab at the University of Cincinnati, Cincinnati, OH.

His research interests include BioMEMS system development with a focus on passive microfluidic systems. He is currently involved in the development of plastic lab-on-a-chip devices for analyzing clinically relevant parameters from human blood.

Jae Y. Lee received the Ph.D. degree in pathology at the College of Medicine, Ohio State University, Columbus, in 1995.

He was with the Yonsei University Hospital and Muhlenberg Hospital, affiliated with Rutgers University, New Brunswick, NJ, as a medical technologist. He was also a Technical Consultant with Glasrock Inc. and an Assistant Professor and Director of the Medical Technology Department for the Ansan #1 University. He is currently a Research Associate with the College of Medicine, Ohio State University. He has several publications in peer-reviewed journals and has also contributed to *Free Radicals in Diagnostic Medicine: A Systems Approach to Laboratory Technologies, Clinical Correlations, and Antioxidant Therapy* (D. Armstrong, Ed., New York: Plenum, 1994). His research interests are the development of point-of-care devices using bioMEMS and finding of cancer markers.

Dr. Lee is a member of the American Society of Clinical Pathologists, the American Association of Clinical Chemists, and the American Association of Medical Technologists.